“STRUCTURAL AND FUNCTIONAL CHARACTERIZATION OF *ESCHERICHIA COLI* FLAVOHEMOGLOBIN”.

ALESSANDRA BONAMORE

Università degli Studi di Roma “La Sapienza”
DOTTORATO DI RICERCA IN BIOCHIMICA - XVII Ciclo
Dipartimento di Scienze Biochimiche “A. Rossi Fanelli”

Coordinatore: Prof. PAOLO SARTI
Dipartimento di Scienze Biochimiche “A. Rossi Fanelli”
Università degli Studi di Roma “La Sapienza”

Tutore scientifico: Prof. ALBERTO BOFFI
Dipartimento di Scienze Biochimiche “A. Rossi Fanelli”
Università degli Studi di Roma “La Sapienza”

Docenti esaminatori: Proff. GIOVANNI ANTONINI, MAURIZIO PACI, NAZZARENO CAPITANIO

Abstract

Flavohemoglobins are oxygen binding proteins composed of a heme-containing globin domain fused with a ferredoxin reductase-like FAD- and NAD-binding domain. Genes codifing for these proteins have been identified in a wide variety of bacteria and eukaryotic microorganisms, although their physiological role is still uncertain. A possible function for flavohemoglobins has been proposed in the framework of the response to nitrosative stress as they are able to catalize the oxidation of free NO to nitrate in the presence of oxygen and NADH.
The aim of this work is to determine the structure of *Escherichia coli* flavohemoglobin (HMP) and to investigate novel possible enzymatic functions for the protein. We have found that HMP is able to bind reversibly a number of unsaturated and cyclopropanated phospholipids and fatty acids as well as liposomes obtained from *E. coli* total lipid extract. Along the same line, HMP is shown to be an efficient alkyl hydroperoxide reductase, thus suggesting that the protein is involved in a specific lipid hydroperoxide repair mechanism induced by oxidative/nitrosative stress.

1. INTRODUCTION

The common perception of hemoglobins and myoglobins as proteins tailored for the transport and storage of oxygen is not adequate to describe the functional properties of globins within all living organisms. In fact, the discovery of globin genes among prokaryotic and eukaryotic microorganisms including bacteria, yeasts, algae, protozoa and fungi rules out the possibility that globin genes were originally designed for oxygen transport or storage. At present, the number of these "hemoglobin-like" proteins is steadily increasing as novel genomes from microorganisms are sequenced and annotated. Such a massive input of newly discovered hemoglobins is revealing an unsuspected and amazingly wide distribution of globin genes within living organisms that are very distant from the phylogenetic point of view. In this framework, within the evolutionary time frame, oxygen transport appears as an emergent function, customized from much older physiological roles, whose nature is under active investigation by the scientific community (Wu et al. 2003, Poole et al. 2000).

1.1 The globin superfamily

Globins can be classified in the framework of a superfamily on the basis of the conservation of the so-called "globin fold", a structural motif made of eight alpha helices (form A to H). Alpha helices are arranged in a globular structure that embeds the heme in a central hydrophobic cavity between helices E and F. As a general rule, globins classification must necessarily be based on structural alignments rather than on simple sequence alignments. This concept was developed by Lesk et al., already in 1987. Upon examination of about 200 globin sequences (from vertebrates, invertebrates and a few plants) and a dozen of tridimensional structures, they pointed out that very few residues are strictly conserved in globins and that the sequence identity between phylogenetically distant globins can be as low as 15%.

All globins are structurally related to vertebrate hemoglobins and myoglobins in that, besides the conservation of the typical globin fold, the heme is always covalently linked to the polypeptide chain through a proximal histidine residue (HisF8) and a Phe residue (PheCD1) appears to be necessary to keep the heme in the correct orientation within the pocket. However, apart from HisF8 and PheCD1, a wide array of different aminoacidic residues can be accommodated within the heme pocket. In fact, several topological positions that are important for the interaction of aminoacid side chains with the iron bound ligand in the distal pocket are not conserved among globins. A typical example concerns the topological position E7, that in vertebrate hemoglobins and myoglobins is a histidine residue but is changed to glutamine in several species. When leaving the world of vertebrate globins to explore the structural features of the (randomly distributed) invertebrate globins, the variability of the aminoacid substitutions within the distal heme site becomes impressive, such that in some nematode hemoglobins none of the distal heme pocket residues is conserved with respect to the aminoacids present in higher vertebrate. Finally, climbing the phylogenetic tree up to unicellular microorganisms, an explosion of different novel (or, more appropriately ancient) globins is observed such that an expansion of the parameters defining the globin family is required. In fact, in many microorganisms, including bacteria, yeasts, algae, protozoa and fungi the classical globin fold is not fully conserved. Microbial globins includes more than a globin family, namely truncated hemoglobins, globin coupled sensors and flavohemoglobins. Globin coupled sensors (GCS) include a number of chimeric proteins in which the globin domain is fused with a transducer domain involved in aerotaxis or gene expression regulation (Freitas et al. 2003). Interstingly, the globin domain of these GCS and in particular the heme containing active site is structurally analogous to the globin domain of flavohemoglobins (Hou et al. 2001). Thus, flavohemoglobins can be considered as a distinct class of chimeric proteins in which the non-globin module is a typical flavodoxin reductase-like domain (Andrews et al. 1992). On the other side, truncated hemoglobins (trHbs) share little sequence

and structure similarity to oxygen sensor domains in that they lack two of the eight helices typical of the globin fold and exhibit a wide array of possible aminoacid substitutions within the active site (Wittenberg et al. 2001). Thus, trHbs have been assigned to a distinct group within the globin superfamily. As a consequence of this multibranched phylogenetic tree, the creation of a globin superfamily that includes these novel microbial globins is currently under development.

Most recently, the presence of ancestral globin genes in thermophilic Archaea has also been demonstrated, thus corroborating the idea that hemoglobins were designed for roles different than oxygen transport in the primordial atmosphere (Wu et al. 2003). The Archaea proteins have been considered as ancestors of bacterial globins and accordingly have been termed *proto*globins (Freitas et al. 2004). Evolution of *proto*globin genes has been suggested to give rise to different globin subfamilies, including flavohemoglobins, whose physiological functions diverged.

1.2 The flavohemoglobin family

Flavohemoglobins are widespread within prokaryotes and eukaryotes although their distribution among different species is apparently hazardous and does not follow a discernable pattern. So far, *Enterobacteriacee* and soil microorganisms all have a flavohemoglobin gene, *Actinobacteriacee* and *Streptomyces* often possess more than a flavohemoglobin and some unicellular eukaryotes (*Candida albicans*) share up to five different genes codifying for flavohemoglobins. The steadily growing input from novel genomes is providing a continuous challenge for the phylogenetic classification of flavohemoglobins such that yearly upgrade of genomic databases includes at least a handful of novel proteins from different organisms. At present, flavohemoglobins have not been identified as yet in strict anaerobes and in Archaea although, as mentioned in the previous paragraph, the presence of single chain *proto*globins displaying a significant structural similarity with the flavohemoglobins heme domain have been reported recently (Freitas et al. 2004).

The flavohemoglobin family is formed by a very homogeneous group of proteins that share highly conserved active sites in both the heme and flavin binding domains. The conserved aminoacids within the heme domain include the residues lining the heme pocket on both the proximal and distal site thus indicating that there must be a strong regio- and stereochemical requirement for ligand binding and/or for gaseous ligand diffusion. In parallel, also the aminoacid residues responsible for flavin binding are strictly conserved and conform to the typical architecture of flavodoxin-reductase proteins indicating clearly that the flavin moiety serves as an electron transfer module from the NADH to the heme. Sequence alignments carried out on separate domains rapidly diverge towards the globin family on one side and on flavodoxin or ferredoxin reductase family on the other thus suggesting that flavohemoglobins have originated from the fusion of a *proto*globin ancestor and a flavin binding domain. Updated sequence alignments and phylogenetic trees have been worked out in the framework of the present thesis and will be presented and discussed in detail.

1.3 *Escherichia coli* flavohemoglobin

The flavohemoglobin from *Escherichia coli* (HMP) has been the first discovered protein of the flavohemoglobin family. Since its identification in 1991, HMP has been object of a large number of investigations aimed to unveil its physiological role and its structural properties.

HMP is encoded by a 1191 bp DNA fragment located at 2683.90 kb in the *E. coli* chromosome. Its promoter overlaps that of the adjacent gly A gene which is however transcribed in the opposite direction. HMP expression is regulated by the FeS protein FNR (fumarate and nitrate reduction), which predominantly functions as a positive transcription factor, though its role of repressor is also important. FNR recognizes a consensus sequence and binds the DNA in response to exogenous signals such as anoxia, redox state, oxidative

and nitrosative stress (Korner et al. 2003). Inspection of the DNA upstream of the hmp reveals two potential FNR-binding sites (Poole et al. 1996). One site, 5'-TTGAG-N_4-ATCAA-3', is centered 34 bp upstream of the hmp translation start codon and closely resembles the consensus sequence, 5'-TTGAT-N_4-ATCAA-3'; its position is consistent with an inhibiting function. A second potential FNR site, 5'-TTGAC-N_4-AGGAA-3' is centered 222 bp upstream of the hmp translation start codon, but has a weaker resemblance to the consensus FNR-binding sequence.

HMP expression seems to be also regulated by Met R. One gene activated by Met R with homocysteine as cofactor is gly A, whose promoter overlaps that of hmp. It has been demonstrated that in *E. coli* elevated homocysteine levels decrease hmp expression (Membrillo-Hernandez et al. 1998). Furthermore, induction of HMP expression was observed in cells entering the stationary growth phase. This induction is mediated by the stationary phase-specific sigma subunit (σ^S) of RNA polymerase (Membrillo–Hernandez et al. 1997).

HMP was first identified in the course of an attempt to discover genes that encode *E. coli* dihydropteridine reductase (DHPR) activities (Vasudevan et al 1991). The authors found a chromosomal DNA fragment that directed the synthesis of two soluble polypeptides of 44 and 46 kDa. The larger protein was serine hydroxymethyltransferase, encoded by the gly A gene, while the smaller was the product of an unassigned gene closely linked to gly A, and divergently transcribed. Soluble extracts of *E. coli* cells that overproduced the 44 kDa protein had elevated DHPR activity. Their visible absorption spectra were indicative of a b-type hemoprotein and the sequence of the N-terminal 139 residues of the protein were highly homologue to *Vitreoscilla* hemoglobin, the first bacterial hemoglobin to be discovered.

In 1992, Andrews and co-workers detected three soluble ferrisiderophore reductases in *E. coli*. One of these was purified and identified as the hemoglobin-like protein (HMP). So far, the protein previously isolated as a dihydropteridine reductase was then shown to have ferrisiderophore reductase activity (Andrews et al. 1992).

Later on, based on the impetus provided by the active and successful research on the biological effects of nitric oxide (NO) and on multiple experimental evidences of an interplay between the NO catabolism and hemoglobin chemistry, it was proposed that HMP might act in connection with a novel NO pathway in bacteria. In particular, HMP was suggested to play a role in the framework of bacterial resistance to nitrosative stress. So far, HMP expression has been demonstrated to respond to the presence of nitric oxide in the culture medium (Hausladen et al. 1998, Membrillo-Hernandez et al. 1999), and an explicit mechanism has been proposed that involves FNR mediated NO induced expression of the flavohemoglobin (Poole et al. 1996, Cruz-Ramos et al. 2002, Corker et al. 2003). HMP has been shown to be able to scavenge and reduce NO to N_2O under anaerobic conditions (Kim SO et al. 1999). In contrast to (or together with) the anaerobic NO reductase activity, HMP has also been shown to be able to catalyze the oxidation of free NO to nitrate (nitric-oxide dioxygenase activity) both in vivo and in vitro in the presence of oxygen and NADH (Gardner et al. 1998). Alternatively, an NO denitrosylase function has been proposed in which, at low oxygen tensions, HMP turns over in the ferric state with the intermediacy of an iron-bound nitroxyl anion that is subsequently transformed into nitrate in the presence of oxygen (Hausladen et al. 2001). It remains to be established which of these diverse enzymatic activities might correspond to a physiologically relevant process. Nevertheless, more recently, other non-heme iron proteins in *E. coli* have been identified that are able to perform NO dioxygenase or reductase activities with a much higher efficiency than flavohemoglobin (Gardner et al. 2003, Gomes et al. 2002, da Costa et al. 2003) thus tuning down the hypothesys of a direct participation of HMP to NO scavenging. The reaction of flavohemoglobin with NO might thus appear simply as a manifestation of the rich and complex chemistry between NO and heme iron rather than a physiologically relevant phenomenon.

1.4 HMP and oxidative stress response

Reactive oxygen species (ROS) are known to be responsible of oxidative damage to macromolecules in vivo and in vitro. Treatments of cells with redox-active drugs may cause lethal damages that involve oxidation of DNA, RNA, membranes and proteins. As a result of the exposure to exogenous ROS generating agents, all aerobic living cells are able to generate O_2^- (or H_2O_2) when molecular oxygen oxides redox enzymes that are designed to transfer electrons to other substrates.

E. coli, as well as most bacteria, respond to oxidative stress by invoking two distinct stress response: the superoxide stimulon and the peroxide stimulon, each containing a set of about 40 proteins, under the control of OxyR and SoxRS systems. These proteins include catalase-peroxidases (katG and katE), superoxide dismutases (sodA and sodB), glutathione synthetase (gshAB), glutathione reductase (gor), endonucleases (nfo, nth), porin (ompF) and alkyl hydroperoxide reductase (ahpC). The signal for the OxyR regulon induction appears to involve the action of H_2O_2 directly, whereas the induction of SoxRS modulon occurs in two steps. An unidentified intracellular signal of oxidative stress changes the conformation of SoxR protein into a transcriptional activator of the soxS gene. The SoxS protein then activates the transcription of genes belonging to the modulone (Amabile-Cuevas et al. 1991). SoxRS system is activated by redox cycling agents (such as paraquat) that generate intracellular superoxide (Farr et al. 1991), and by nitric oxide (Nunoshiba et al. 1992).

As previously reporter, HMP itself is responsive to nitric oxide, but unlike other NO-induced genes, the induction of HMP is SoxRS independent. Besides, it has been observed that HMP is able to generate superoxide radicals and H_2O_2 (Membrillo-Hernandez et al. 1996), acting as an amplifier of superoxide stress and leading to the full expression of SoxRS stress response.

A novel set of functional hypotheses pertaining the involvement of HMP in the oxidative stress response has been inferred on the basis of structural studies based on X-ray diffraction and resonance Raman spectroscopic investigations. In particular, X-ray crystallographic studies carried out on similar proteins, namely *Alcaligenes euthrophus* flavohemoglobin (FHP) and the single chain hemoglobin from *Vitreoscilla sp* (VHB), pointed out that the structural geometry of the active site was strongly reminiscent of that of typical peroxidases. The 3D structure of VHB and FHP revealed that the proximal heme pocket is characterized by a network of hydrogen-bonding interactions that comprises the Nε atom (hydrogen-bonding donor) of the proximal histidine, thus conferring an anionic character to the imidazole ring (Tarricone et al. 1997, Ermler et al. 1995). The spectroscopic signature of the peroxidase-like character of the active site has been provided by resonance Raman measurements on the fully reduced, deoxygenated HMP derivative whose spectrum displays a very high iron histidine-stretching frequency, in line with the values observed for typical peroxidases (Mukai et al. 2001). Subsequently, infrared absorption measurements conducted on the cyanide-bound ferric species confirmed the structural analogies between HMP and peroxidases highlighting the strong electron donation to the iron-bound ligand (Bonamore et al. 2001). These features can be taken as a central structural motif that allows to distinguish between genuine hemoglobins, in which the integrity of the ligand in the trans position needs to be preserved, and peroxidases, in which electron donation to the trans oxygen ligand up to the cleavage of the O-O bond is at the core of the catalytic activity (electron push effect). Moreover, the presence of both a glutamine and a tyrosine (Tyr B10) in the distal site of the heme pocket suggested that these two residues might well play the same role as the His-Gln couple in typical peroxidases.

These last observations, indicating that HMP may be endowed with peroxidase and/or monooxygenase activities, represent the starting point of the present work.

1.5 Biotechnological applications of bacterial hemoglobins

It is of interest that, despite the poorly understood physiological role, the biotechnological applications of bacterial hemoglobins have exploded in a myriad of industrial processes, in particular in bio-oxidative transformations (Minas et al. 1998, Nasr et al. 2001, Urgun-Demirtas et al. 2003, Lin et al. 2003, Khang et al. 2003). The presence of recombinant bacterial hemoglobins within the host cell has been shown to promote the growth rate and increase cell density of the transformed cells even under oxygen limiting conditions, to improve the bio-oxidation product yield, to alleviate oxidative and nitrosative stress during the stationary phase and ameliorate both heterologous enzymes expression and their catalytic capabilities (Bollinger et al. 2001, Frey et al. 2000, Frey et al. 2002, Kim YK et al 2004). Thus improved *E. coli* vectors expressing bacterial hemoglobin-like proteins are routinely used in several bioreactors and large fermentors. The observed beneficial effects of bacterial hemoglobins have been initially attributed to a facilitated oxygen delivery to oxidizing enzymes, including the terminal oxidases of the host cell (Park et al. 2002, Kallio et al. 1994). This hypothesis has been challenged on the basis of the extremely slow rate of oxygen release characteristic of bacterial hemoglobins, a phenomenon that rules out facilitated oxygen diffusion (Giangiacomo et al. 2000).

1.6 Aim of the work

The aim of this work is to determine the structure of *Escherichia coli* flavohemoglobin and to investigate novel possible enzymatic function for the protein. HMP is thought to be involved in the response of bacterial cell to the potentially harmful role of free nitric oxide in giving rise to the nitrosative stress. Nevertheless, although the nitric oxide dioxigenase stands as the major functional hypothesis for HMP, a number of experimental observations carried out on highly similar proteins have revealed different possible scenarios for bacterial hemoglobins' functions. In particular, the structural resemblance of the heme environment of flavohemoglobins with classical peroxidases suggested the participation of these proteins to some sort of peroxidase-like activity towards some unknown substrate. Recently, different kind of bacterial hemoglobins have been demonstrated to interact with membrane phospholipids both in vivo and in vitro. In fact, *Alcaligenes eutrophus* favoemoglobin has been crystallized with a tightly phospholipids within the heme pocket and *Vitreoscilla* hemoglobin, as well as *Mycobactrerium tuberculosis* truncated hemoglobin, has been reported to be preferentially located in contact with the bacterial inner membrane in vivo and to be capable of reversible binding to liposomes in vitro.

In this framework, the interaction of HMP with heme ligands and with membrane lipids will be investigated and possible enzymatic activity involving membrane phospholipids will be screened.

2. MATERIALS AND METHODS

2.1 MOLECULAR BIOLOGY METHODS

2.1.1 Cloning and expression of HMP

The hmp gene encoding for the *Escherichia coli* flavohemoglobin was amplified from the bacterial genomic DNA. A Polymerase Chain Reaction has been performed using the Vent Polymerase (Biolabs), the forward primer 5'-GGAAGACCATATGCTTGACGCTC-3' which contains a Nde I restriction site and the reverse primer 5'-CGGGTCAATCGGATCCGTACCGG-3' 70 base pairs downstream the stop codon, which is cut by BamH I.

A PTC-150 Mini Cycler Hot Bonnet apparatus (MJ Research, inc.) was used to carry out the gene amplification. The PCR mix had the following composition: 100 ng genomic DNA, 50 pmol forward primer, 50 pmol reverse primer, 250 µM dNTPs, 1.6 units Vent Ploymerase, 1X Vent buffer and 50 µl deionized water. The amplification steps, 1 minute at 95°C, 1 minute at 65 °C, 1 minute and 30 seconds at 72 °C, were repeated 30 times. The PCR product was loaded onto an agarose gel, analyzed by electrophoresis and extracted from the agarose using a QIAquick Gel Extraction Kit (QIAGEN).

hmp and the expression vector pET 11-a (Novagen) were cut with both Nde I and BamH I, purified and ligated. The ligation reaction was performed using Ready-To-Go T4 DNA ligase (Amersham Pharmacia biotech).

Escherichia coli k12 BL21 (DE3) made competent to be transformed through $CaCl_2$ treatment were transformed with the ligation mix and the clones containing the plasmid pET 11-hmp were selected by their ability to grow in plates in the presence of ampicillin.

One of these clones was growth in LB liquid medium supplemented with 100 mg/l of ampicillin for about 16 hours. Afterwards 60 mg/l of δ-aminolevulinic acid (ALA) were added and after another 30 minutes the HMP expression was induced by adding 1mM IPTG. 4 hours later the cells were recovered by centrifugation.

2.1.2 Cloning and expression of the mutant

The GluH23-Val mutant of HMP was obtained by making use of site-directed mutagenesis by whole plasmid synthesis (WHOPS). This method is based on the capability of certain DNA polymerase to be used for the synthesis of entire plasmid, using a pair of complementary primers, which introduce the point mutation. In our case the mutant sense primer is 5'-GGCTAATGTATTTATCAATCGCGtGGCGGAAATCTATAACGAAAAGC-3' and the mutant antisense primer is 5'-CGTTTTCGTTATAGATTTCCGCCaCGCGATTGATAAATACATTAGCC-3'.

pET11-hmp plasmid used as WHOPS template was isolated from a Dam methylation competent strain (DH5α). The PCR mix was as following: 100 ng plasmid DNA, 0.5 µM mutant sense primer, 0.5 µM mutant antisense primer, 250 µM dNTPs, 1X polymerase buffer, 2.5 units Pfu turbo polymerase (Fermentas), 50 µl deionized water. The PCR cycle was 45 seconds at 95 °C, 1 minute at 68 °C, 4 minutes at 70 °C for 16 times. 10 units of the restriction enzyme Dpn I were directly added to the PCR reaction, so that the methylated template which did not carry the mutation could be digested. This mix was then used to transform BL21 (DE3) strains. The introduction of the mutation was confirmed by DNA sequencing.

To express the mutant protein we used the same protocol described for the wild type HMP.

2.1.3 Cloning and expression of the heme domain

The HMP heme domain was cloned in a the pET-11a plasmid. pET 11-hmp vector was chosen as template for PCR amplification. Vent DNA polymerase was used with the

primer pairs forward 5'-GAAGACCATATGCTTGACGCTC-3' and reverse 5'-GCGAGTAGGATCCTAACGACGACGACGGCTGGCGTTTTCG-3'. The reverse oligonucleotide was drown adding 4 arginine codons, 1 stop codon and a restriction site for Bam HI at the end of the H helix of the heme domain. The 470 bp product was isolated from an agarose gel and digested with both Nde I and Bam HI. The product was then purified and ligated in the pET-11a plasmid, cut with the same restriction enzymes. The ligated product was transformed into *Escherichia coli* BL21 (DE3) strain and the clones containing the plasmid were selected by their ability to grow in the presence of ampicillin. A recombinant plasmid screening was then performed using a control PCR and confirmed by DNA sequencing.

HMP heme domain has been expressed as reported previously for the full length protein.

2.2 PREPARATIVE BIOCHEMISTRY METHODS

2.2.1 HMP extraction and purification

E. coli flavohemoglobin, cloned and overexpressed in *E. coli*, was purified by means of a three-steps chromatographic procedure that avoids amoniun sulfate precipitation and yields ≥ 5 mg of pure protein per liter of culture. The *E. coli* crude extract was loaded onto a DEAE 52 column equilibrated with 10 mM Tris-HCl buffer at pH 8 containing 0.1 mM EDTA, 1 mM dithiothreitol and 1 mM potassium cyanide. The flavohemoglobin was eluted with an NaCl gradient at 0.18 M salt concentration. The fraction with flavohemoglobin higher than 50 %, as judged by SDS-PAGE, were pooled, dialyzed against 5 mM phosphate buffer at pH 7 and loaded onto a microceramic hydroxyl-apatite (Bio-Rad, Hercules, CA, USA) column equilibrated with the same buffer. A 5-50 mM phosphate gradient (pH 7.0) was applied and the protein eluted at a buffer concentration of 15 mM. The fractions containing more than 90 % flavohemoglobin were directly loaded onto a DEAE-Toyo Pearl (Toso Haas) column equilibrated with 15 mM phosphate buffer and eluted with an NaCl gradient (0-0.25 M). The protein obtained was 98 % pure on SDS-PAGE and was fully saturated with flavin cofactor as judged from the ratio (0.27) between the absorption peak of the heme cyanide complex (419 nm) and the oxidized flavin peak (480 nm).

The flavohemoglobin concentration was determined spectrophotometrically using a molar absorptivity of 156000 M^{-1} cm^{-1} at 419 nm for the ferric cyanide derivative.

2.2.2 Extraction and purification of the HMP GluH23-Val mutant

HMP mutant overexpressed in *E. coli* is not fully saturated with the heme cofactor. For this reason the protein has been reconstituted with hemin, dialyzed against phosphate buffer 20 mM pH 7 and then loaded onto a G-25 gel filtration column. Afterwards the mutant was purified as previously described for the native protein.

2.2.3 Extraction and purification of the heme domain

The HMP heme domain was purified by using the first two chromatographic steps used in the whole HMP purification, i.e. a DEAE 52 column and a microceramic hydroxyl-apatite column. An easier purification was feasible owing to the four C-terminal arginine residues, that increased the isoelectric point of the heme domain with respect to the other *E. coli* proteins.

2.2.4 Phospholipids extraction and manipulation

Total *E. coli* lipid extracts (TLE) were prepared according to Bligh and Dyer (1959). Briefly, 250 mg of *E. coli* pellets obtained after sonication and centrifugation of whole cells were washed with deionized water, dried under vacuum at -5 °C and dissolved in 5 ml of a

methanol/chloroform (2:1 v/v) solution. The solution was vortexed at room temperature and stored at 4 °C for 24 hours. Thereafter, the sample was centrifuged at 6000 rpm, the supernatant was kept at 4 °C and the pellet was subjected to a new extraction procedure as before. Then, 5 ml of chloroform and 5 ml of water were added to the chloroform methanol supernatants, the chloroform phase was separated, dried under nitrogen gas at 4 °C and stored at -20 °C. The effective removal of protein components from the lipid extracts was checked by IR spectroscopy (absence of the 1650 cm^{-1} amide band).

Fatty acids methyl esters (FAME) from *E. coli* total lipids were obtained with a single-step (extraction-transesterification) method (T. Lewis et al., 2000). 50 mg of freeze-dried cells were put into a screw-top test tube, suspended in 3 ml of the transesterification mix (methanol:hydrochloric acid:chloroform (10:1:1 v/v/v)), and paced at 90 °C. After about an hour, the tube was removed from heat. 1 ml of water was then added and the FAME extracted (hexane:chloroform, 4:1 v/v, 3x2 ml). For gas chromathographic (GC) analysis, the sample was dried and suspended in absolute hexane.

2.2.5 Crystallization procedures

Crystallization experiments were carried out at 25 °C using the sitting drop vapor diffusion method. A volume of 4 µl of protein sample (22 mg/ml) in water was mixed with an equal amount of the reservoir solution containing 0.1 M sodium acetate buffer, pH 5.1-5.3, 21-26 % PEG 3350 and 0.2 M NaCl. Crystals grew in one week to about 0.05 mm × 0.05 mm × 0.1 mm.

Data were collected as 0.5 oscillation frames on the ELETTRA beamline at Basovizza (Trieste) at a wavelength of 1.0 Å and at 100 K using 26 % PEG 200 as cryoprotectant. Data analysis, performed with DENZO (Otwinowski et al. 1997) indicates that the crystals are hexagonal P622 with cell dimensions a=b=164.86 Å, c=53.46 Å, α=β=90°, γ=120°. Heavy atoms derivatives were generated by soaking crystals in reservoir solution plus 5mM $Hg(CH_3COO)_2$ (36 h), or 5mM K_2PtCl_4 (48 h).

2.3 ANALYTICAL BIOCHEMISTRY METHODS

2.3.1 High Pressure Liquid Chromatography

HPLC has been used to screen the activity of HMP towards cumyl hydroperoxide. A 5 ml solution containing 5 µM HMP, 5 mM NADH, and 2.2 mM cumyl hydroperoxide in 0.1 M phosphate buffer was equilibrated under nitrogen for 1 hour at 25 °C. A protein-free blank was also prepared under the same condition. The reaction was quenched by the addition of 5 ml of ethyl acetate and 2 mM benzyl alcohol was added as internal standard. The organic phase was recovered and split in two phases. The first sample was dried under vacuum and resuspended in methanol for HPLC analysis. The methanol solutions (blank and sample) were injected onto an Agilent 1100 Series HPLC system equipped with a Supelcosil LC-18DB (25 cm × 2 □m) reverse phase HPLC column. The products were eluted with 30% v/v methanol/water solution at a flow rate of 0.5 ml/min and monitored at 256 nm.

2.3.2 Gas Chromatography/Mass Spectrometry

The reaction products obtained from the cumyl hydroperoxide in the presence of HMP were also analysed by GC/MS. In fact, since the organic phase of HMP-cumyl hydroperoxide reaction becomes poor in benzyl alcohol (internal standard) after drying under vacuum, part of it was directly used for GC analysis. GC analysis was carry out using a Varian CP-3800 gas chromatographic apparatus equipped with a CP-Sil 5 CB column (30 cm × 0.25 mm) in the following conditions: 10 min at 40 °C, 7°C/min up to 250 °C, 10 min at 250 °C.

2.3.3 Electrospray Ionization Spectrometry

For ESI mass spectrometry measurements, linoleic acid hydroperoxide or its reaction products were extracted as follows: the reaction mixture (1 ml) containing 2 □M HMP in 0.1 M pH 7.0, 1mM EDTA and 20 % v/v ethanol, 140 □M linoleic acid hydroperoxide and 500 □M NADH was allowed to stand 15 minutes under a nitrogen gas atmosphere at 25 °C. At the end of the reaction, the solution was treated with 2 ml of ethylacetate, vortexed and centrifuged at 6000 rpm for 15 minutes. Two blank solutions were prepared in which either NADH or HMP were omitted. The ethylacetate extracts were dried under vacum and resuspended in 80% ethanol/water containing 0.5% v/v ammonia. The ethanolic solutions were analyzed by infusion (5 □l/min) in an electrospray ion trap mass spectrometer (ES-IT, mod. LCQ, ThermoFinnigan, San Jose, CA, USA). Linoleic hydroperoxide standards, dissolved in the same solvent, were used to optimize the ESI source parameters. The mass spectra were collected over the mass range of 70-700 a.m.u., in negative ion mode.

2.3.4 Gel filtration analysis

Gel filtration experiments were carried out according to Chiancone et al. (1974). A Sephadex G-75 (Pharmacia, Uppsala Sweden) column (0.5×35 cm) was used at a constant flow rate of 5 ml/h and at 20 °C. All experiments were carried out in 50 mM phosphate buffer at pH 7.0. 0.2 ml of a protein solution (25 □M) were applied on the column and the elution profiles was monitored in the Soret region with a Jasco 7800 spectrophotometer equipped with a thermostatted flow cell. Column calibration was determined by using native human hemoglobin tetramer (carbonmonoxy derivative) and horse heart myoglobin. Liposomes were obtained from dried TLE resuspended in 10 ml of 50 mM phosphate buffer at pH 7.0, heated at 60 °C for 15 minutes and then sonicated in a Soniprep 150 sonicator for 30 minutes. The liposomes thus obtained were left 4 h at 4 °C, pelleted by centrifugation and resuspended in buffer before use. Phospholipid content in TLE was determined by FTIR absorption of the carboxyl ester at 1735 cm^{-1} on a weighted amount of dry TLE dissolved in chloroform with respect to a phosphatidylethanolamine standard (Sigma Aldrich Co.). Liposome solutions (0.4 ml) containing 20:1 phospholipid/protein molar excess were mixed with 0.1 ml of HMP solutions (25 □M) and then applied on the G-75 column. Horse Mb (Sigma Aldrich Co.) was also run in gel filtration experiments in the presence of TLE as a control.

2.3.5 UV-Visible and near infrared absorption spectroscopy

Absorption spectra were recorded either on a Jasco V-570 spectrophotometer (Jasco Ltd, Japan) or on a Hp 8452 diode array spectrophotometer. Single crystal spectra were measured with a 4DX ray System AB microspectrophotometer (Wilmot et al. 2002).

2.3.6 Resonance Raman spectroscopy

The experiments were carried out in the lab of prof. Giulietta Smulevich at the Department of Chemistry, University of Florence. Resonance Raman (RR) spectra were obtained at room temperature with excitation from the 406.7 nm line of a Kr^{+} laser (Coherent, Innova 302). The back-scattered light from a slowly rotating NMR tube was collected and focused into a computer-controlled double monochromator (Jobin-Yvon HG2S) equipped with a cooled photomultiplier (RCA C31034A) and photon counting electronics. RR spectra were calibrated to an accuracy of 1 cm^{-1} for intense isolated bands with indene as the standard for the high-frequency region and with indene and CCl_4 for the low-frequency region.

2.3.7 X-ray absorption spectroscopy

Fe K-edge X-ray absorption spectra of lipid-free and lipid-bound HMP were collected in fluorescence mode at the BM30-B (FAME) beam line of the ESRF synchrotron facility. The HMP samples were in 1:3 glycerol-water solutions buffered at pH 7 (50 mM phosphate).

The final iron concentration was 4mM and the spectra were collected at 40 K. The met-myoglobin (aquo-MetMb) solution was 7 mM (heme) in the same buffer. The storage ring was running in the 2/3 filling mode with a typical current of 170 mA. The monochromator was equipped with a Si (111) double crystal, in which the second crystal was elastically bent to a cylindrical cross section. The energy resolution at the Fe-K edge is 0.5 eV. The X-ray photon beam was vertically focused by a Ni-Pt mirror, and dynamically sagittally focused in the horizontal size. An array detector made by 24 Ge elements of very high purity was used. For each sample 10 spectra were recorded with a 7s/point collection statistic and averaged. The spectra were calibrated by assigning the first inflection point of the Fe foil spectrum to 7111.2 eV.

2.4 LIGAND BINDING STUDIES

2.4.1 Ligand binding equlibria

Titration experiments were carried out by adding small volumes of imidazole (Sigma Aldrich Co.) solutions to the protein solution (8 □M) in 0.1 M sodium phosphate buffer at pH 7.0 and 20 °C in a 1 cm quartz cuvette. Imidazole titration experiments were carried out on both lipid free and lipid (UFA, CFA or TLE) saturated ferric protein.

2.4.2 Ligand binding kinetics

2.4.2.1 Lipid binding to ferric HMP

Purified, lipid free protein has been screened for heme visible absorption spectral changes against a number of phospolipids (dipalmitoil phosphatidil choline, dipalmitoil phosphatidil ethanolamine, dipalmitoil phosphatidic acid), saturated (palmitic and stearic), unsaturated (oleic, palmitoleic, linoleic, *cis* vaccenic) and cyclopropanated (9,10 methylen palmitoleic) fatty acids and their methyl esters, aromatic hydrocarbons (benzene, toluene, naftalene), linear and cyclic alkenes (1 dodecene, 6 dodecene, cyclohexene, cyclooctene). The screening was performed on 8-12 □M protein solutions in 0.1 M phosphate buffer at pH 7.0 and 20 °C containing 20 % v/v ethanol by adding increasing amounts of ligand (1 to 100 molar excess) dissolved in ethanol. All reagents were from Sigma Aldrich Co. with the exception of cyclopropan palmitoleic acid (Larodan Fine Chemicals, Malmö, Sweden).

Fatty acid binding kinetics were performed by mixing 5 □M HMP in 0.1 M phosphate buffer at pH 7.0 and 20 °C containing 20 % v/v ethanol with a solution containing increasing amounts of palmitoleic, cyclopropanpalmitoleic or linoleic acid, dissolved in the same buffer, in an Applied Photophysics stopped flow apparatus (Leatherhead, U.K.). Fatty acid release kinetics were estimated in competition essays with the lipid avid hydroxylalkoxypropyl-dextrane resin (Tipe X, Sigma Aldrich Co.). 5 ml of a gel suspension containing 20 mg of dried resin in 0.1 M phosphate buffer at pH 7.0 and 20 % v/v ethanol were placed in a small beaker under stirring at 20 °C. The fiber optic “Dip Probe” of a Varian Cary 50 spectrophopometer, equipped with a 150 W pulsed Xe lamp, (Varian Instrument Co. Australia) was immersed in the suspension and a baseline was recorded. A HMP solution (100 □l, 160 □M) saturated with oleic, cyclopropan-palmitoleic or linoleic acid was then added to the suspension and spectra were measured in sequential mode (9 s for each spectrum). Fatty acid release was monitored by following the spectral changes in the Soret region.

2.4.2.2 Imidazole binding to ferric HMP

Ligand combination kinetics of imidazole were carried out by mixing the lipid free or TLE saturated protein solutions (6-8 □M) with imidazole solutions in an Applied photophysics rapid mixing apparatus (Applied Photophysics, Leatherhead, UK).

In order to single out the rate constants of Schemes II (see Results, Fig. 16), the following procedure was adopted: i) only the spectral transitions involving imidazole binding or release to the heme site are considered to contribute to the observed signal; ii) the set of imidazole combination time courses were fitted to the Scheme II by fixing the equilibrium thermodynamic constants to the values obtained in the imidazole titration experiment. In this fitting procedure it was assumed that the intramolecular process determined by K_3 is much faster with respect to the other processes. Hence, four rate constants, namely k_1, k_2, k_4 and k_5 were allowed to float. The total □ absorbances were fixed, for each time course, to the equilibrium values. The Matlab 5.0 program (The Math Works Inc. South Natick, MA) was used in all least squares fitting procedures.

2.4.2.3 Ligand binding to ferrous HMP

Oxygen release kinetics were carried out according to the oxygen pulse method (Boffi et al. 2004). Briefly, the protein solutions containing 10-50 mM sodium dithionite were mixed with oxygen containing buffer. Oxygen binding to the heme iron occurs within the dead time of the instrument (4 ms) and is subsequently released due to the rapid reaction of oxygen itself with dithionite to produce higher sulphur oxides. Thus, the observed spectral signal pertains to the formation of deoxy heme and is monitored at the relevant Soret peak around 434 nm or at 415 nm (the peak of the oxygenated species). Slower absorbance changes (a decrease at 434 nm and an increase at 420 nm) were observed over tens of minutes time scale and were attributed to the binding of some dithionite byproducts to the heme iron and the subsequent formation of a hemochrome-like species. Such effects are dithionite concentration dependent and are negligible up to 50 mM dithionite. It was also observed that aged protein solutions (frozen at -70 °C for three months) exhibited almost complete hemochrome formation within few minutes from dithionite addition. On the basis of these observations, oxygen pulse experiments were carried out on freshly prepared protein and were shown to be fully reproducible in different preparations up to 50-100 mM dithionite.

The CO binding kinetics of HMP were measured in oxygen free solutions at pH 7.0 (0.1 M phosphate buffer), in the presence of 1 mM EDTA and 250 □M NADH, and 20.0 °C by laser photolysis. The HMP solution containing NADH was accurately degassed in a tonometer until the fully deoxy species is formed. Thereafter, the solution was equilibrated with CO gas at 20 °C to a final equilibrium concentration of 1 to 0.025 mM. The measurements have been carried out using as an optical pump the second harmonic from a Quanta System Nd-YAG laser (□= 532 nm, frequency of 2 Hz with pulse width of 5 ns and pulse energy of approximately 80 mJ). The laser pulse flashes the sample in a tonometer with a fluorescence quartz cell of 1 cm length orthogonally to the optical probe due to a 100 W UV-visible source focused onto a monochromator SPEX 1681. Single wavelength measurements have been acquired using as detector a photomultiplier tube Hamamatsu H6870. The time courses (average of 64 traces) were recorded using a digital oscilloscope Tektronix TDS 360. The time courses were followed at 434 nm, as a function of CO concentration (ranging between 1 and 0.025 mM) at a protein concentration of 4 □M.

2.4.2.4 Enzyme kinetics

Enzyme kinetic measurements were carried out by mixing anaerobic protein solutions containing 250 mM NADH and 1 mM EDTA with solutions containing different concentrations of tert-butyl, cumyl, linoleic acid hydroperoxides (13(S) hydroperoxy 9Z,11E octadecadienoic acid) or hydrogen peroxide (Sigma Aldrich Co.) in an Applied Photophysics rapid mixing apparatus equipped with a diode array device (Leatherhead, UK). Stock solutions of tert-butyl, cumyl and linoleic acid hydroperoxide were prepared in 50% water/ethanol mixtures, degassed in a tonometer and kept at 4 °C in the dark before use. Solutions containing HMP and NADH and solution containing hydroperoxides were accurately degassed in a tonometer and anaerobically transferred to stopped flow syringes.

The syringes containing HMP and NADH were allowed to stand for 5 minutes before mixing in order to ensure the consumption of residual oxygen. Double mixing experiments were also carried out in the same stopped flow apparatus: NADH (250 μM) reduced HMP (8 μM) was first mixed with H_2O_2 in the pre-mixing chamber and, after a 2 s delay, with 20-1000 □M CO (oxygen free) solutions. Alternatively, slower kinetic time courses at low protein concentrations (below 1 □M) were carried out by mixing the NADH reduced protein with the alkylhydroperoxide solutions directly in a tonometer equipped with a 1 cm quartz cuvette and a side arm reservoir. In CO inhibition experiments, a few □l of a CO gas saturated solution were added to the tonometer with a microsyringe and equilibrated for 20 min with the acqueous phase before adding the substrate to yield an equilibrium CO concentration of 1-20 □M. Time courses were followed at 340 nm (absorption maximum of NADH) on a Jasco V-570 spectrophotometer. All experiments were carried out in 0.1 M phosphate buffer at pH 7.0 containing 1 mM EDTA and at 25 °C. In the case of linoleic acid hydroperoxide, reaction kinetics were carried out in the presence of either 0.1 % Triton X-100 or 20 % v/v ethanol/water mixture.

3. RESULTS

3.1 ANALYSIS OF THE THREE DIMENSIONAL STRUCTURE

3.1.1 The overall fold

The overall fold of HMP (Fig. 1) consists of heart shaped structure in which three different domains, namely the C-terminal NAD-binding domain, the FAD-binding domain and the N-terminal globin domain are clearly distinguished.

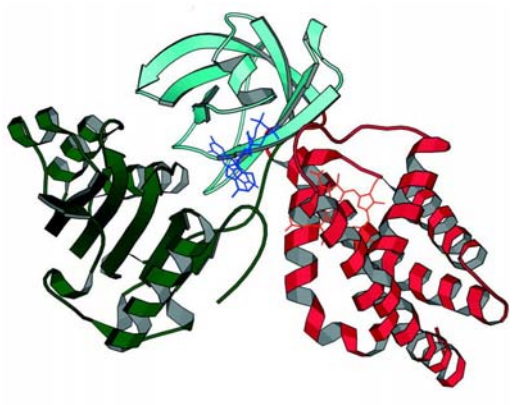

Fig. 1 Overall structure of *Escherichia coli* ferric unliganded flavohemoglobin. The heart shaped structure is positioned with the flavin binding domain at the upper apex (cyan), the globin domain on the lower right side (red) and the NAD-binding domain on the lower left side (green) (panel A). The ribbon diagram was depicted using the program MOLSCRIPT

The tridimensional structure of HMP is compared to that of *Alcaligenes eutrophus* flavohemoglobin (FHP), formerly obtained by Ermler et al. (1995). In spite of the high degree of sequence similarity between HMP and FHP, the superposition of the two structures obtained with the program Spdb viewer, results in a high root mean square deviation (6.83 Å). Such a deviation is due mainly to a rotation of the NAD-binding module (see Fig. 2, panel A) and to a substantial rearrangement of the E helix positioning within the globin domain in HMP with respect to FHP. It is important to point out that the HMP structure has been obtained on the fully oxidized protein (i.e. heme-iron in the ferric state and oxidized flavin), whereas the structure of FHP was determined on the fully reduced protein (i.e. heme-iron in the ferrous state and reduced flavin).

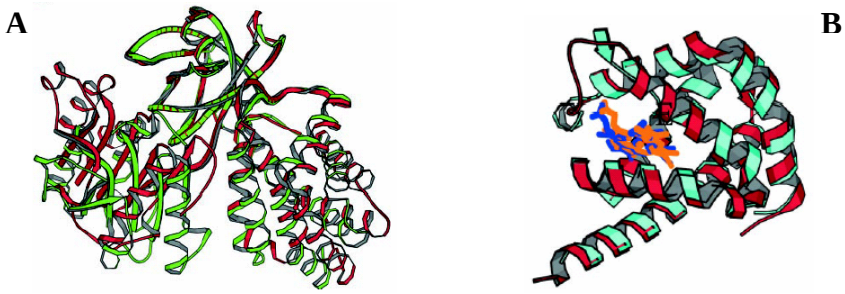

Fig. 2 Structural overlay of the globin domains of *Escherichia coli* and *Alcaligenes eutrophus* flavohemoglobin and *Vitreoscilla* sp. hemoglobin.
The overlay among globin domains was obtained by minimizing the Cα distances for each protein using the program Spdb viewer. The stereo diagram of the globin domain of HMP (red ribbons, yellow heme) is overlayed with the corresponding domain of *Alcaligenes* eutrophus flavohemoglobin (green ribbons, green heme) in panel A and with *Vitreoscilla* Hb (cyan ribbons, blue heme) in panel B.

3.1.2 The globin domain.

The architecture of the globin domain corresponds to a classical globin fold composed of eight helices (from A to H) with an unusually long H helix and in which the D helix is substituted by a large loop region within the segment CD2-E6 (Asn44 to Asp52). Apart from the invariant residues PheCD1 and HisF8, considered as the hallmark of the globin structure, the heme pocket geometry show little resemblance to that observed in vertebrate hemoglobins and myoglobins. Inspection of the distal pocket architecture reveals that the distal position, closest to the iron atom, is occupied by the Leu57 (E11) isopropyl side chain with the CG atom at 3.6 Å distance from the iron atom along the normal to the heme plane (Fig. 3). Leu-E11 side chain together with the Phe-CD1 ring, the Ile61 (E15) and Val98 (G8) side chains and the Gln53 (E7) backbone segment, fill completely the first distal shell (Fig. 3). In contrast, Tyr29 (B10) and Gln-E7 side chains, previously proposed as the major candidates for iron-ligand distal stabilization (Peterson et al. 1997, Ermler et al. 1995), are shifted from the heme at a distance of more than 5.0 Å. The Tyr B10 phenol ring is confined to the second layer of distal pocket residues with the phenol hydroxyl pointing towards the isopropyl chain of Leu E11.

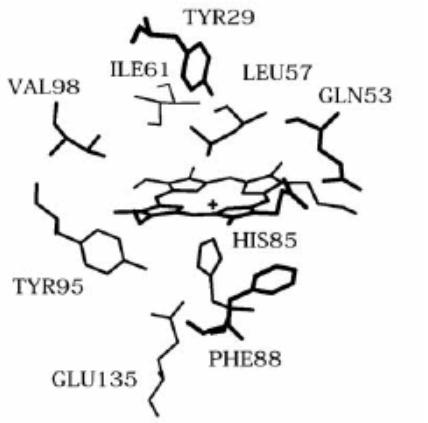

Fig. 3 Structural details of the heme pocket in *Escherichia coli* ferric unliganded flavohemoglobin.
The heme molecule is shown together with a selection of aminoacid residues within the pocket at 5 Å from the macrocycle. The phenolic ring of Tyr29 (B10), located at more than 5 Å form the heme, is also shown whereas the Phe43 (CD1) is hidden for clarity. The picture was obtained with the program MOLSCRIPT.

The architecture of the heme pocket in the proximal region is characterized by the presence of the canonical proximal histidine (His F8) residue whose Nδ atom coordinates the ferric heme iron at 2.01 Å distance. However, at variance with vertebrate hemoglobins, the proximal histidine is involved in a hydrogen bonding network between His85 (F8), Tyr95 (G5) and Glu135 (H23) (see Fig. 3) that imparts a rigid orientation to the imidazole histidine ring with respect to the heme plane. In particular, the OE2 atom of Glu135 is involved in a hydrogen bonding interaction at 2.9 Å from the ND1 nitrogen of the proximal histidine. In turn, Glu135 is anchored to the phenol hydroxyl of Tyr95 by a hydrogen bonding (OE2 at 2.7 Å from the Tyr oxygen atom).

Another peculiar structural feature of the HMP heme domain consists in the arrangement of the CE loop region. In fact, as shown in Fig. 4, the cavity formed by the residues Asn44-Asp52 is filled with a strong electron density whose electronic shell most likely pertains to a large anion such as chloride or phosphate. Possible electrostatic interactions to the bound anion have also been identified and include a positively charged ammonium ion belonging to residues Arg49, amide nitrogen of Asp52 and Arg54 and/or to the O2D oxygen atom of a heme propionate.

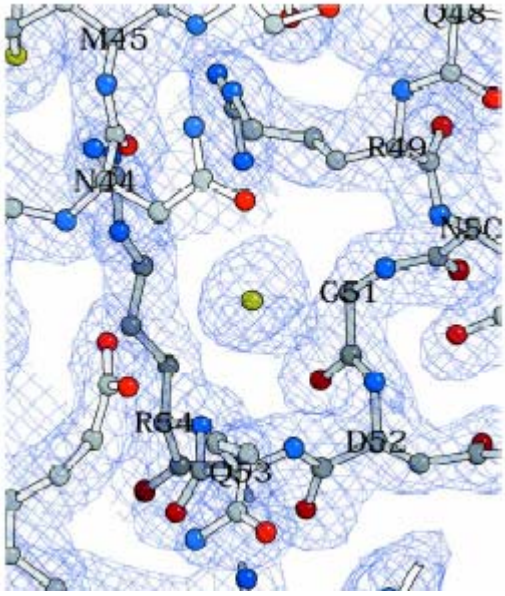

Fig. 4 Electron density map of the CE region of *Escherichia coli* heme domain.
Electron densities were calculated with the program XPLOR (Brünger et al. 1992) and contoured at 1σ from the residues A44-A56. The anion residing at the center of the map was tentatively assigned to a chloride ion (yellow sphere).

This finding is of particular interest due to the location of the loop on the heme edge towards the propionate region and in contact with the flavin binding module. A possible functional implication of the anion binding site in modulating the heme ligand binding properties will be discussed later.

3.1.2.1 Comparison between E. coli and A. eutrophus globin domain.

The structural overlay of the Cα skeleton of HMP and FHP globin domains indicates that a major difference between the two proteins pertains to the positioning of the E helix that is shifted far from the heme plane in the latter protein (Fig. 2A). The structural overlay between the two proteins demonstrates clearly that in FHP heme domain the E helix shift is determined by the accomodation of a bulky phospholipid molecule that alters the positioning of the relevant distal pocket residues (Ollesch et al 1999). In particular, in FHP, the cyclopropane ring of a 9,10-methylen-hexadecanoic chain of a dyacylglycerol-phosphatidic acid (a common fatty acid component within the bacterial membranes) sits on the top of the iron atom apparently displacing the relevant distal site residues. In fact, in FHP, Leu-E11 accompanies the lipid induced E helix movement and is displaced by 4.6 Å away from the heme pocket with respect to its positioning in HMP. Interestingly, HMP is also capable of binding membrane lipids, although with lower affinity with respect to FHP (Ollesch et al. 1999) and VHB has also been recently reported to be able to interact with the bacterial inner membrane (Ramandeep et al. 2001). Taken together, these observations suggest that lipid binding is not a distinctive feature of FHP but may represent a common property of the bacterial hemoglobin family, the functional role of which is still to be defined.

3.1.2.2 Comparison between HMP heme domain and Vitroscilla Hb.

The striking similarity of the overall fold of the heme domain in HMP and Vitreoscilla Hb (Cα structure superposition rmsd = 1.58) shown in Fig. 2B, is not reflected in a similar architecture of the distal heme pocket in that notable differences concern the nature and/or the geometry of the E8 and E11 topological positions. The proline ring in position E8 in VHB lies close to the heme plane normal at 3.8 Å from the metal in the distal pocket (Tarricone et al. 1997), but is substituted by an arginine residue in HMP whose side chain is oriented outside the distal pocket. Leu-E11, in HMP, occupies a genuine distal site position along the normal to the heme plane whereas the same residue, in VHB, is in a staggered conformation and appears to line the edge of the heme (Tarricone et al. 1997, Bolognesi et al. 1999). In both

HMP and VHB the Gln E7 side chain does not contribute to the formation of the first distal pocket shell in the unliganded derivatives.

3.1.2.3 The FAD binding domain

The structures of the FAD- and NAD-binding modules in HMP are superimposable to those observed in FHP. The former consists of a six-stranded antiparallel β-barrel with Greek key topology capped by a helix at the bottom and an irregular peptide at the top. The latter is built up of a five-stranded parallel β sheet flanked by two helices on the one side and by one helix and an irregular structural element on the other. The FAD-binding and NAD-binding domains are fused to build the so-called oxidoreductase module, which structurally belongs to the ferredoxine reductase family.

Nevertheless, two major differences between HMP and FHP need to be considered further. First, as shown in Fig. 2A, the relative orientations of the FAD- and NAD-binding domains in the two proteins differ. In particular, the entire NAD-binding domain in HMP is rotated clockwise with respect to the relative orientation observed in FHP thus leading to a considerably larger interdomain cleft in HMP. The second point concerns the structural arrangement of the isoalloxazine binding motif. The *si*-side geometry is strikingly similar in the two proteins in that the segment 205-207 (207-209 in FHP) and the Tyr188 (190 in FHP) exhibit identical orientations with respect to the isoalloxazine plane (see Fig. 5). Other conserved contacts (not shown) to

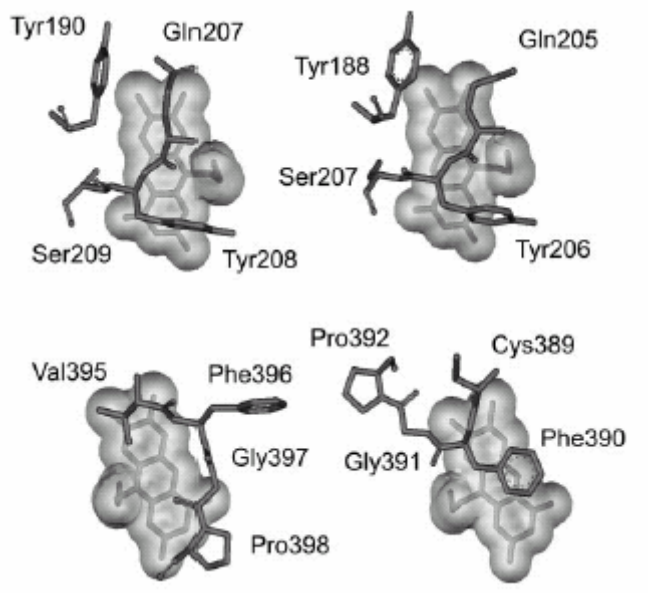

Fig. 5 Structural details of the FAD binding site in *Escherichia coli* ferric unliganded (right) and *Alcaligenes eutrophus* ferrous, lipid bound (left), flavohemoglobins.
The isoalloxazine three membered ring (embedded in a transparent Van der Waals surface) is shown together with a selection of aminoacid residues located within 5 Å distance from the macrocycle atoms in the *re*-side (top) and in the *si*-side (bottom). Pictures were obtained with the program ViewerLite.

the flavin moiety involves Val269 in HMP (276 in FHP) and Thr272 (279 in FHP). In contrast, the *re*-side, that faces the C-terminus loop region of the NAD-binding domain, is quite different in the two proteins. In fact, in HMP, the aromatic ring of the conserved Phe390 (396 in *A. eutrophus*) is packed against the isoalloxazine central ring whereas in FHP it protrudes towards the interdomain cleft. Considering the high sequence similarity within the FAD- and NAD-binding domains of the two proteins, both the rotation of the NAD-domain

and the differences in the *re*-side of the isoalloxazine binding motif may be suggestive of a conformational change linked to the binding of a phospholipid molecule. Thus, it may be envisaged that the lipid free species is stabilized by a stacking interaction of the isoalloxazine ring with Phe390 (in HMP) whereas, upon lipid binding (*i.e.* in FHP), the whole C-terminus loop is shifted and rotated towards the ribitol moiety with concomitant loss of the stacking interaction. In spite of these significant structural rearrangements, the relative positioning of the isoalloxazine moiety and the heme plane are superimposable in the two proteins and only a modest decrease in the closest distance between the two cofactors is observed (the distance between the C8AF atom of the isoalloxazine and OA1 of the heme propionate is 6.3 Å in FHP and 5.9 Å in HMP).

3.2 ALIGNMENTS

More than 50 putative flavohemoglobins have been identified trough a BLAST research on bacterial and eukaryotic genomes. A phylogenetic analysis of these proteins has been performed using CLUSTAL W (1.75) Multiple Sequence Alignment as shown in Fig. 6.

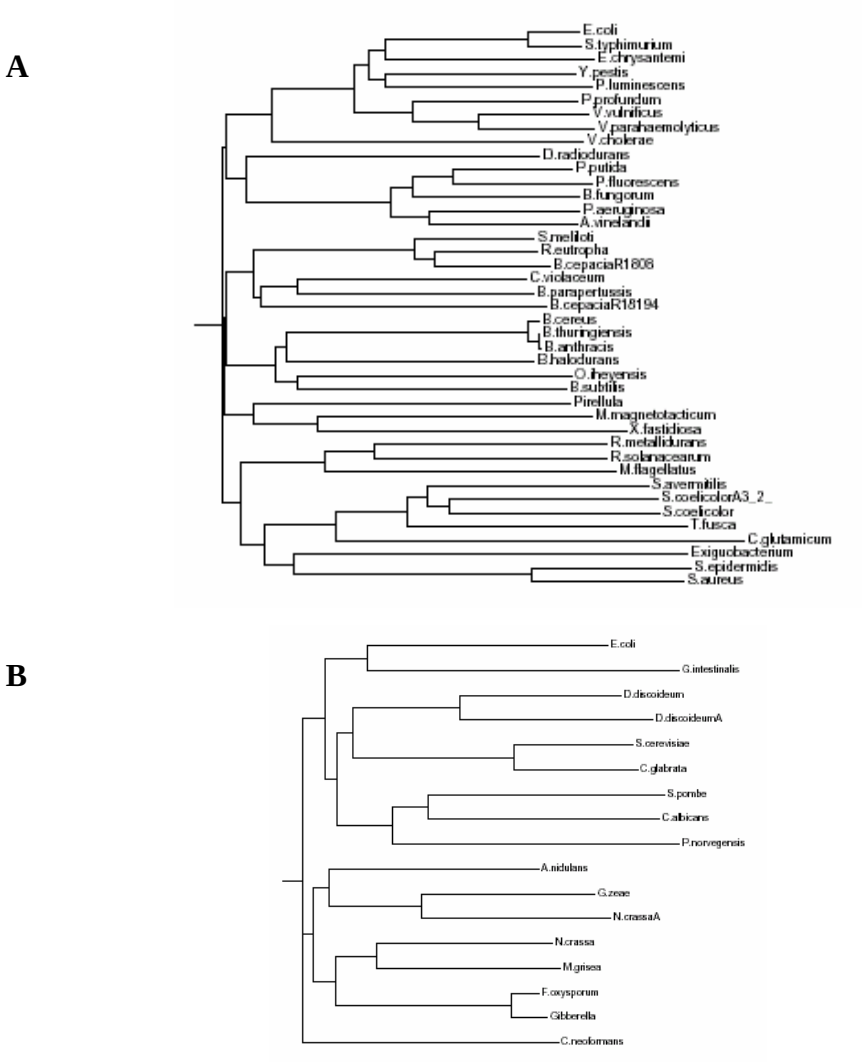

Fig. 6 Phylogenetic trees showing the relationship among flavoHbs.
The distance trees have been constructed aligning HMP with bacterial (panel A) and eukaryotic (panel B) flavohemoglobins using CLUSTAL W (1.75) Multiple sequence alignment . The program is freely available at http://www.es.embnet.org/cgi-bin/clustal.cgi.

There is a number of aminoacids that are strictly conserved among all these proteins within both the heme and the FAD binding domains (Fig. 7).

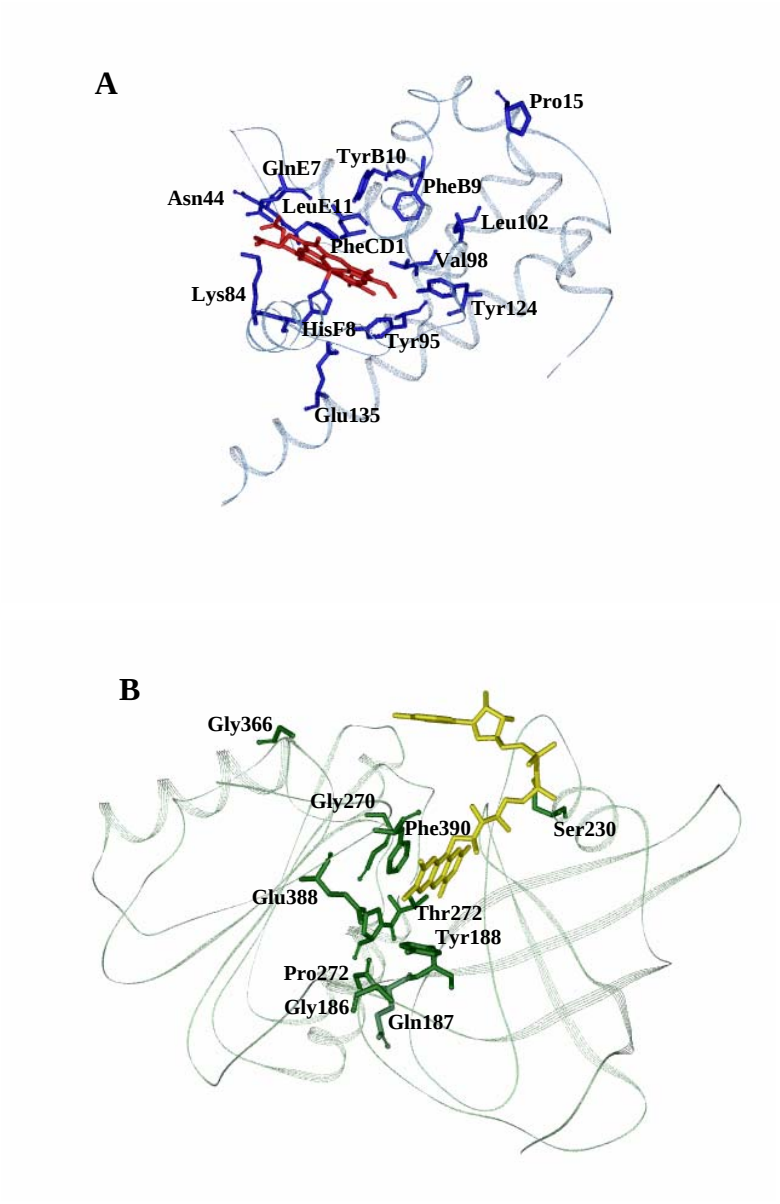

Fig. 7 Conserved residues within the flavohaemoglobin family.
HMP heme domain (panel A) and flavin domain (panel B) are shown. The stick pictured aminoacids represent residues conserved among all flavohemoglobins identified so far. Pictures were obtained with the program ViewerLite.

Invariant residues close to the heme cofactor correspond to Phe28 (B9), Tyr29 (B10), Phe43 (CD1), Gln53 (E7), Leu57 (E11), Asn44, Val98, Leu102 and Tyr124 on the heme distal side and His85 (F8), Glu135, Tyr95 and Lys84 on the heme proximal side of *Escherichia coli* flavohemoglobin. Phe43 is absolutely conserved in all species and its aromatic side chain binds nearly parallel to the heme plane. The proximal histidine (His F8) is also invariant in all known globin sequences, even if its environment changes remarkably. Within the flavohemoglobin family this histidine is hydrogen bond to the conserved Glu135 and Tyr95. The distal Tyr29 and Gln53 are supposed to be involved the stabilization of the oxygen bound to the heme iron. Finally, Phe28, Leu57, Val98 and Tyr124 seem to be involved in phospholipid binding.

The conserved aminoacids of the flavin domains correspond to residues: Phe290, Gly270, Glu388, Thr272, Pro273, Gly186, Gln187, Tyr188 and Ser23. These residues occupy topological positions that are highly distinctive of ferredoxin (or flavodoxin) reductases, a

subfamily of flavin binding proteins that is highly specialized in electron transfer from the NADH cofactor to the flavin moiety and to a high redox potential electron acceptor, tipically a ferredoxin. Consistently, the conserved residues appear to contour and shape the flavin binding cavity thus reducing solvent access and providing the structural basis for the interaction with NADH as a substrate.

3.3 LIPID BINDING PROPERTIES

The interaction of bacterial Hbs with membranes has been first proposed for *Vitreoscilla* Hb, that has been demonstrated to bind the inner membrane and act as a facilitator of oxygen transfer by placing it closest to respiratory chain. *A. eutrophus* flavohemoglobin is also able to bind phospholipids as observed in the X-ray structure that shows, adjacent to the heme molecule, an unexpected electron density originally designated as an unknown ligand (Ermler et al. 1995). Later, the nature of this ligand was identified as a phospholipids (Ollesch et al. 1999). The X-ray structure of HMP not only revealed a high degree of similarity with the VHB and FHP, but also showed that the aminoacids involved in the binding of the lipid are strictly conserved.

On the basis of these data, the fatty acids and phospholipids binding properties of HMP in solution were investigated both by thermodynamic and kinetic methods.

3.3.1 Gel filtration analysis

We have shown that *Escherichia coli* flavohemoglobin is able to bind reversibly a number of unsaturated and cyclopropanated phospholipids and fatty acids (UFA and CFA) as well as liposomes obtained from *Escherichia coli* total lipid extracts (TLE). HMP binding to different types of liposomes was tested by means of gel filtration chromatography. The elution profiles reported in Fig. 8 were obtained by measuring the absorption of the G-75 column elute at the HMP Soret peak (405 for the ferric derivative and 420 nm for the CO bound ferrous derivative). The peak at 8.22 ml corresponds to the void volume as measured by dextran blue (profile 1). Liposomes are also eluted within the void volume as demonstrated by the slight absorbance increase around 8.3 ml (profile 5). Experiments carried out with freshly prepared TLE liposomes and horse Mb (ferric) indicated that the protein does not interact with the membranes and that no heme is released to the lipid bilayer under the present experimental conditions (profile 2). In apparent contrast, Ramandeep et al. (Ramandeep et al. 2001) reported a weak but detectable interaction of both horse Mb and human hemoglobin with bacterial membranes. However, their size exclusion measurements were at equilibrium, (*i.e.* there was no mobile solvent phase through the gel matrix) whereas the present classical gel filtration experiment implies that even interacting particles (*i.e.* liposomes and Mb) can be sieved depending on their molecular mass if their interaction is weak. Thus, the present experiments cannot exclude a weak interaction between Mb and lipid bilayers. Moreover, heme release from ferric Mb to liposomes has been shown to be negligible at pH 7.0 and 20 °C whereas it does occur at pH values below 5.0 and temperature higher than 25 °C (unpublished data). In turn, the elution profile of HMP in the presence of TLE liposomes (profile 3) displays two separate peaks at 8.3 and 11.7 ml respectively, whose integrated surfaces account for 55% and 45 % of the total area. The peak at 8.3 ml contains both the TLE liposome fraction and ferric HMP whereas the peak at 11.7 corresponds to the elution volume of free HMP. The absorption spectra of the two fractions, shown in panels *a* and *b* of Fig. 8, correspond to the spectrum of ferric, lipid bound, HMP (see also Fig. 9). The gel filtration data indicate clearly that HMP is not only capable of strong binding to liposomes obtained from *E. coli* lipid extracts (TLE) but may also abstract phospholipids from the liposome fraction, although it cannot be excluded that free, monodisperse lipids might be present in the liposome preparation even after centrifugation. Mass spectrometric analysis performed on the second fraction revealed the presence of heterogeneous phospholipid species. The nature of

the bound phospholipid, however, cannot be assessed with certainty due to the intrinsinc heterogeneity of the *sn-1* and *sn-2* glycerol linked components. As a control, purified, lipid free HMP was also screened towards dipalmitoil phosphatidil choline vescicles and only a negligible interaction has been detected (profile 4).

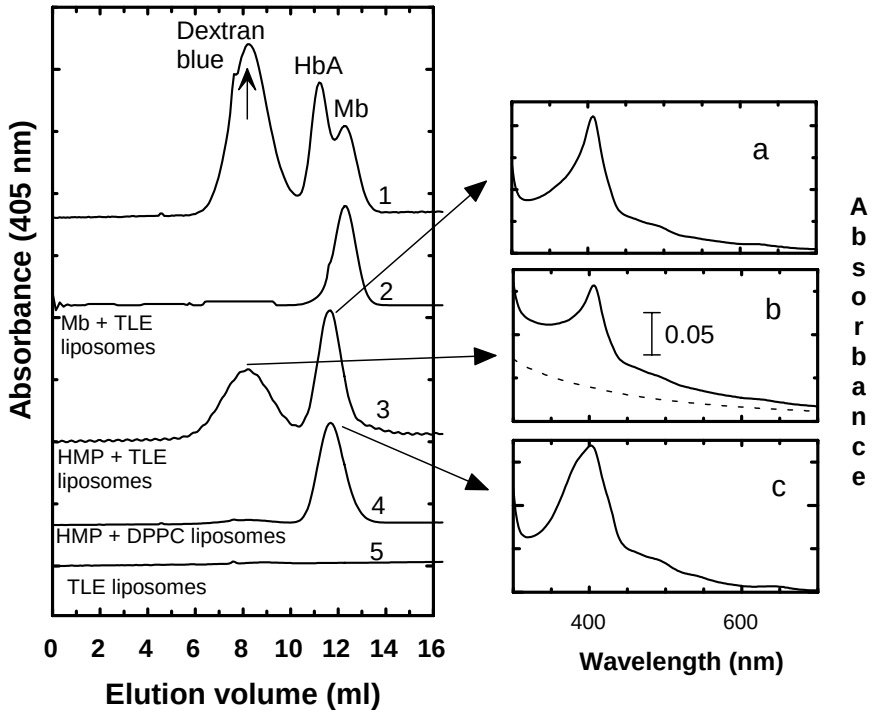

Fig. 8 Elution profiles of *E. coli* flavohemoglobin on a gel filtration column in the presence of liposomes. From top to bottom: standard solution composed of of blue dextran (the arrows correspond to the excluded volume), carbonmonoxy human hemoglobin (HbA) and horse heart myoglobin (Mb) (profile 1); ferric Mb mixed with total lipid extracts (TLE) from *E. coli* cells (profile 2); purified ferric unliganded HMP mixed with liposomes (20:1 phospholipid/protein molar ratio) obtained from *E. coli* total lipid extracts (profile 3); purified ferric unliganded HMP mixed with DPPC liposomes (20:1 phospholipid protein molar ratio) (profile 4); TLE liposomes (profile 5). The absorption spectra of the eluates relative to profiles 3 and 4 are also shown in panels a, b, and c, respectively. Experiments were carried out on a G-75 Sephadex column equilibrated with 50 mM phosphate buffer at pH 7.0 and 20 °C.

3.3.2 Spectroscopic properties.

In order to gain full understanding of the complex relationship between HMP and phospholipids the structural nature of protein-lipid interactions need to be explored. Nevertheless, in spite of considerable efforts, crystallization of lipid bound HMP could not be achieved under the experimental conditions in which the lipid free derivative easily yields a number of small hexagonal crystals. For these reasons the fine structural aspects of HMP-lipid interaction have been investigated by means of EXAFS, resonance Raman and UV-Vis spectroscopy.

3.3.2.1 UV-Vis absorption spectra of the lipid bound derivative

The present investigation originated from the observation of spectral changes in ferric HMP noticed during the protein purification procedure and initially attributed to the loss of flavin from the holoprotein. In particular, the visible absorption spectra of HMP before and after hydroxylapatite chromatography were different (see below). Electrospray mass spectrometry, performed on the protein before hydroxylapatite chromatography, revealed the

presence of heterogeneous protein-linked components attributed to phosphatidyl ethanol amine and phosphatidic acid derivatives, in full agreement with the report by Ollesch et al. (1999). Further inspection on the fatty acid methyl esters obtained from HMP-bound phospholipids shows the nature of the estherified fatty acids, that are palmitic acid and C16 or C18 unsaturated or cyclopropanated chains.

In Fig. 9 the unliganded and linoleic acid bound derivatives are shown. The absorption spectra of the unliganded derivatives display a broad Soret band, characterized by a low molar absorptivity and centered at 403 nm. In the visible region, a prominent charge transfer band (CT 1) is observed at 645 nm both in solution and in the crystal. The solution spectra of HMP saturated with free unsaturated fatty acids or phospholipids displays a sharp peak at 407 nm and a CT 1 at 625 nm. This last spectrum was superimposable to that observed in the ferric protein before hydroxylapatite chromatography thus providing evidence that bound phospholipids are removed by this chromatographic step. The spectral changes observed upon lipid binding or release were also reproduced upon removal of the lipid species by means of hydrophobic chromatography (hydroxyalkoxypropyl-dextrane) thus demonstrating that the lipid binding is fully reversible.

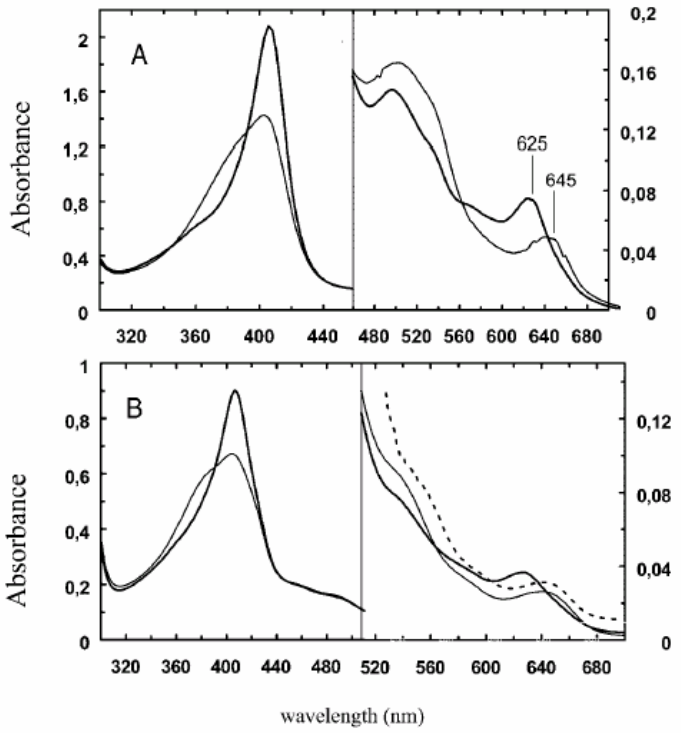

Fig. 9 UV-Visible absorption spectra of ferric *Escherichia coli* flavohemoglobin and its heme domain.
The spectra of the ligand free (thin line) and linoleic acid bound (thick line) HMP heme domain are collected in panel A. The spectra of the ligand free (thin line) and linoleic acid bound (thick line) full length HMP are collected in panel B together with the spectrum of ligand free HMP in the crystal (dashed line). All spectra are in 0.1 M phosphate buffer at pH 7.0.

3.3.2.2 RR spectra of the lipid bound derivative

RR spectra reported in Fig. 10 have been obtained on the HMP heme domain. Full length HMP could not be safely analyzed with the 406.7 nm excitation due to the strong flavin absorption at this wavelength and hence to the possible photoreduction of the flavin itself. The RR high frequency region (Fig. 10, panel B) in which coordination and spin state marker bands are apparent is almost identical to that obtained by Mukai et al. (2001) on the full length protein. It displays the typical features of a ferric, high spin, pentacoordinate derivative with a υ_3 band at 1492 cm^{-1}, a υ_2 peak at 1567 cm^{-1} and υ_{10} at about 1630 cm^{-1}

overlapped with vinyl stretching modes at 1623-1630 cm^{-1}. Upon linoleic acid or TLE binding (spectra b and c, respectively) the core size marker bands shift to 1478 cm^{-1} (υ_3), 1560 cm^{-1} (υ_2) and 1606 cm^{-1} (υ_{10}). In addition, a band at 1516 cm^{-1} is clearly observed (υ_{37}). These frequencies correspond to those observed for six coordinate, high spin, heme iron complexes (Spiro 1985). The low frequency region (Fig. 10, panel A) displays intriguing spectral features in that lipid binding is accompanied by a strong enhancement of the 319 cm^{-1} peak with a shoulder at 305 cm^{-1}. These bands are observed at the same frequencies both with linoleic acid and with TLE phospholipids (containing mainly cyclopropanated fatty acids) thus indicating that they do not likely originate from an iron ligand stretching mode. Thus, the 319 cm^{-1} and 305 cm^{-1} bands are tentatively assigned to the γ_6 and γ_7 out of plane modes of the heme skeleton in analogy with myoglobin whose frequencies are observed at 337 and 305 cm^{-1}, respectively (Hu et al. 1996). However, their enhancement in the spectra of the hexacoordinate high spin heme iron is unexpected since these modes are known to be preferentially RR active in distorted hemes, such as pentacoordinate heme (Smulevich et al. 1996).

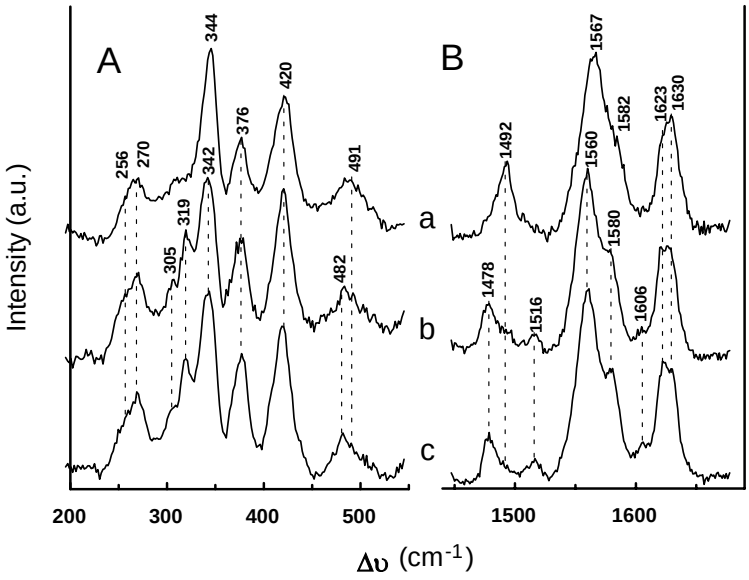

Fig. 10 Resonance Raman spectra of ferric *Escherichia coli* flavohemoglobin heme domain.
Spectra in the high frequency (panel A) and low frequency (Panel B) region of lipid free ferric HMP (a), linoleic acid bound HMP (b) and TLE saturated HMP (c). The protein concentration was 90 μM in (a) and (b) and 35 μM in (c). Buffer was 0.1 M phosphate buffer at pH 7.0. Experimental conditions: 16 mW laser power at the sample, 5 cm^{-1} resolution. The accumulation interval ranges from 4 s / 0.5 cm^{-1} to 16 s / 0.5 cm^{-1}.

3.3.2.3 EXAFS spectra of the lipid bound derivative

The Fourier transform (FT moduli) of the EXAFS spectra corresponding to lipid free HMP, (HMP_LF, solid curve), lipid bound HMP (HMP_LB, dashed curve) and aquo-MetMb (dotted curve), extracted with a cubic spline, are shown in Fig. 11, lower panel. The FTs have been calculated in the interval k = 3.2-10.0 $Å^{-1}$ with no phase-shift correction applied. The spectral intensity (absorption) are plotted as a function of R, which represents the distance from the scattering element (i.e. from the iron 2p electron shell) and thus reflects the distance among the iron atom and the nearby nuclei within about 4 Å.

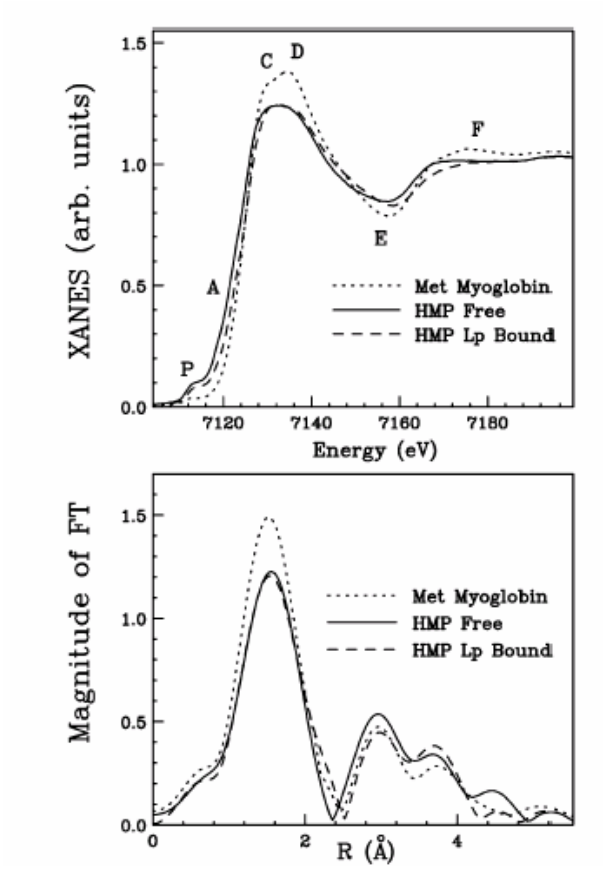

Fig. 11 Fe K-edge XANES spectra of *Escherichia coli* flavohemoglobin. Upper panel: Normalized Fe K-edge XANES spectra of lipid free HMP (full line), lipid bound HMP (dashed line) and met-myoglobin (dotted line). Lower panel: Fourier transforms of the lipid free HMP (full line), lipid bound HMP (dashed line), and met-myoglobin (dotted line) EXAFS experimental spectra calculated in the range k= 3.2-10.0 $Å^{-1}$ using a Hanning window.

Thus, the high intensity peaks around R=1.5 Å are associated with the atoms from the first coordination shell around the iron atom. In the case of lipid free HMP it comprises four pyrrolic nitrogen atoms of the porphyrin ring (N_p) and one nitrogen atom of the proximal histidine (N_h). An additional oxygen atom contributes to this peak in the case of aquo-MetMb. The second set of peaks, between R values of 2 and 3.5 Å contain all the single and multiple scattering contributions associated with the carbon atoms in the second coordination shell of both the porphyrin plane and the proximal histidine. According to the crystallographic structure, the distal site of the heme iron in HMP is occupied by the isopropyl side chain of the LeuE11. Therefore, two additional carbon atoms of this residue contribute to the second peak of the lipid free HMP FT spectrum at about 3.5 Å. The third set of peaks beyond 3.5 Å is mainly due to the single and multiple scattering contributions associated with the third shell of the tetrapyrrole macrocycle atoms.

Simple inspection of the EXAFS spectra offers interesting insight into the structural changes that accompany lipid binding to HMP. It can be noticed that both the position and intensity of the first EXAFS peaks of liganded and unliganded HMP are identical. However, the right-hand shoulder of the first EXAFS peak is increased and the amplitude of the second peak at R = 3 Å is decreased in the liganded derivative. All together these observations indicate that a structural change of the Fe environment occurs at the axial site in the presence of the lipid within a R value in the range 2.5-3.5 Å. Data analysis showed that a binding interaction occurs between the ferric heme iron and a couple of atoms located at 2.7 Å from the metal indicating that the ferric heme is clearly hexacoordinated. Nevertheless, inspection of the crystal structure of the ferrous, lipid bound, *A. Eutropus* FHP (1.75 Å resolution) indicates that the iron-nearest carbon atom (CA of the cyclopropane ring, see Fig. 12) in ferrous, lipid bound, FHP is at 3.5 Å distance from the metal. Such distance precludes any bonding interaction between the iron atom and the distal ligand in that no orbital overlap can be predicted to occur involving the dz^2 ferrous or ferric iron orbital at a distance higher than

3.0 Å. Interestingly, the ferric, ligand free, HMP displays similar structural features within the iron first coordination shell with the CG carbon atom of LeuE11 at 3.4 Å distance from the iron atom. Thus, in ferrous lipid bound and ferric lipid free flavohemoglobins, the iron atom preserves a pentacoordinate stereochemistry and establishes no bonding interactions at the distal site.

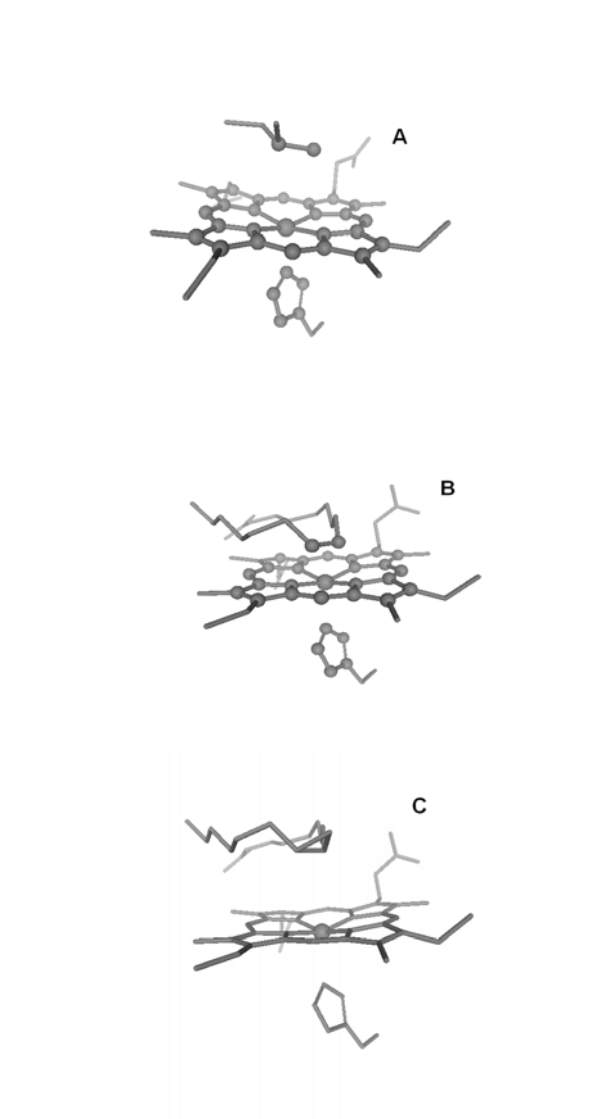

Fig. 12 Heme iron coordination geometry in flavohemoglobins.
The crystal structure of the active site of ferric, lipid free *Escherichia coli* flavohemoglobin (PDB code:1GVH; panel A) is compared with the structure of the ferrous cyclopropanpalmitoleic bound *Alcaligenes eutrophus* flavohemoglobin (PDB code:1CQX; panel C). The hypothetical structure of ferric, linoleic acid bound HMP is shown in panel B. The atoms belonging to the cluster used in EXAFS and XANES data analysis are shown as spheres.

3.3.2.4. Spectroscopic properties of the mutant GluH23-Val

The UV-vis absorption spectra of a mutant in which the glutamate 135 involved in an hydrogen bond with the proximal histidine (see above) is substituted by the apolar valine, is superimposable to the spectra of the native HMP. The mutant overespressed in *E. coli* is purified in the lipid bound form, which is stable even after the hydroxyl apatite chromatography step.

Further investigations in the far infrared region show that the charge transfer band at 760 nm (band III), typical of five coordinate high-spin ferrous heme (Chavez et al. 1990), is centred at 758 nm in HMP and shifted at 762 nm (Fig. 13) in the mutant.

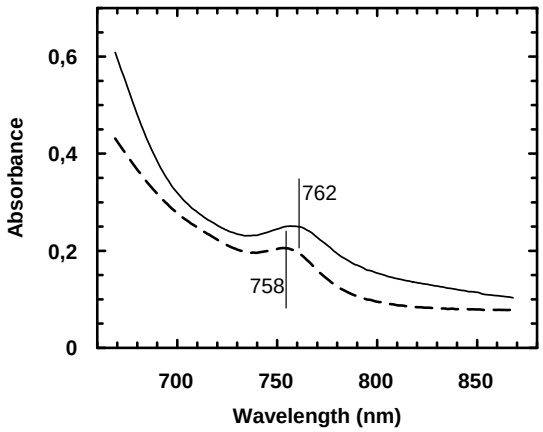

Fig. 13 Far infrared spectra of native HMP and HMP GluH23-Val.
Spectra in the far infrared region of dithionite reduced native HMP (full line) and of HMP GluH23-Val (dotted line). Band III at 760 nm is shift at 762 nm in the mutant.

3.3.3 Lipid binding kinetics

HMP was shown to interact with bacterial lipid membranes and to be able to bind specifically phospholipids and fatty acids within the heme pocket. As previously mentioned, lipid binding is associated with spectroscopic transitions in the EXAFS, resonance Raman and UV-vis. A fully reversible spectral transition is observed upon mixing the purified protein with total bacteria lipid extracts, but also with simple UFA and CFA free acids (see Fig. 14).

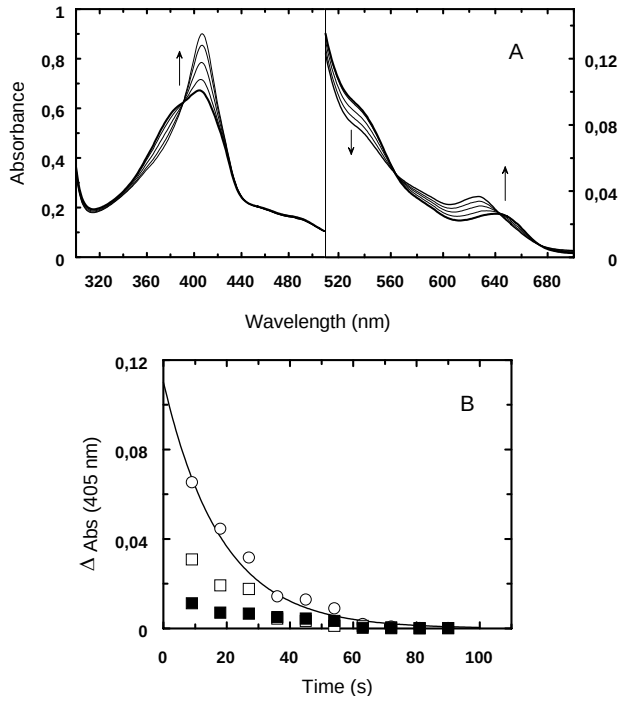

Fig. 14 Spectral changes in the UV-Vis absorption region accompanying lipid binding to ferric *E. coli* flavohemoglobin and kinetics of lipid release.
A stoichiometric titration of lipid free, ferric HMP (12 μM heme) with an ethanol solution of oleic acid (3 μM per each addition) is shown in panel A. Panel B reports the kinetics of linoleic (○), oleic (■) and cyclopropan-palmitoleic (□) acid release from HMP as obtained in competition essays with hydroxyalkoxypropyl-Dextrane. The continuous line represent the monoexponential fit to the linoleic acid data obtained by imposing the total absorbance change (at t=0) to the calculated value ($k = 5 \pm 2.2 \times 10^{-2}$ s^{-1}). All experiments were carried out in 50 mM phosphate buffer at pH 7.0 in the presence of 20 % v/v ethanol at 20 °C.

Subsequent titrations, carried out in buffers containing 20% v/v ethanol, pointed out that UFA and CFA bind to HMP with an extremely high affinity, even when the protein is pretreated with saturated fatty acids and/or saturated phospholipids. In order to strengthen the correlation

between fatty acids binding and observed spectral signal and to estimate a value for the apparent affinity constant, a set of ligand combination kinetics were carried out by rapid mixing experiments. In these measurements, ferric HMP (in 20% ethanol) was mixed with increasing concentrations of palmitoleic, cyclopropanpalmitoleic and linoleic acid under pseudofirst order conditions. The time courses of linoleic acid binding to HMP as a function of wavelength and lipid concentration are reported in Fig. 15. The time courses were collected into a data matrix and processed by a Singular Value Decomposition (SVD) analysis in order to single out possible spectral intermediates. However, the procedure did not allow for an unequivocal deconvolution of the data set and eventually served to remove noise from the observed time courses. Fitting the (SVD) averaged time courses to single exponentials resulted in slightly biased time courses thus indicating that a more complex process than simple second order binding underlines the lipid binding process to HMP. Fatty acid concentrations higher than 0.1 mM could not be obtained due to solubility problems and thus, a full pseudo first order plot could not be produced. The apparent second order rate constant obtained from the fitting of the data of Fig. 15 C is around 2×10^{6} M^{-1} s^{-1} (see also legend of Fig. 15). Palmitoleic and cyclopropanpalmitoleic acids displayed time courses 6-7 fold faster than linoleic acid and their kinetic parameters could not be estimated with certainty. A rough estimate of the lipid release rate was obtained by competition essays of lipid bound HMP with hydroxyalkoxypropyl-dextrane. The results obtained, shown in Fig. 14 B, indicate that palmitoleic and cyclopropanpalmitoleic acids are rapidly released from HMP ($k > 0.1$ s^{-1}, assuming first order release). In contrast, linoleic acid dissociates with an apparent rate of 5×10^{-2} s^{-1} thereby fixing the apparent affinity constant to a value of about 4×10^{7} M^{-1} (in the presence of 20 % ethanol).

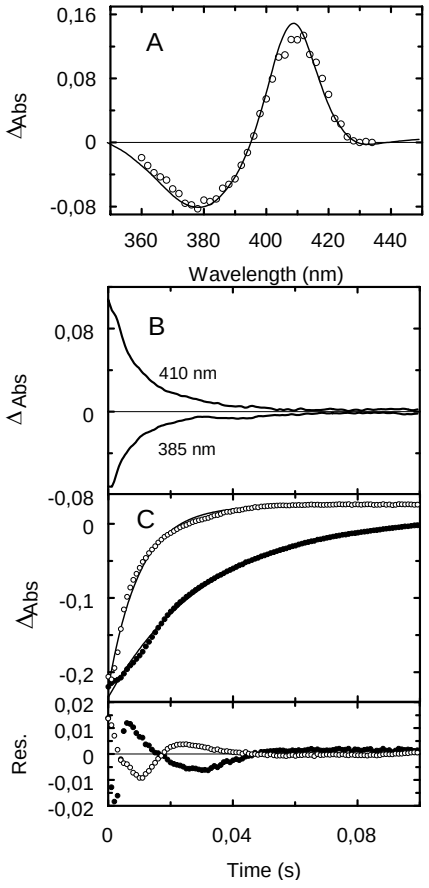

Fig. 15 Kinetics of linoleic acid combination to ferric *E. coli* flavohemoglobin.
Panel A shows the static (continuous line) and kinetic (○) difference spectra in the Soret region of linoleic acid bound ferric HMP minus lipid free ferric HMP. Time courses, as obtained in rapid mixing experiments at two selected wavelengths, are shown in panel B. The kinetics records obtained at all wavelengths were collected into a data matrix and averaged by standard procedures (see Experimental Procedure). The averaged traces are shown in panel C together with single exponential fitting curves (continuous lines) and residuals. Apparent pseudo first order rates were 105 and 31 s^{-1}, respectively. Experimental conditions were: protein concentration (after mixing), 5 μM; linoleic acid concentrations (after mixing), 5×10^{-5} M (○) and 2.5×10^{-5} M (●); 0.1 M phosphate buffer, pH 7.0 containing 20 % ethanol and 20 °C.

3.4 HEME-LIGAND BINDING PROPERTIES OF HMP

In order to compare the reactivity of the heme domain to that of other vertebrate and invertebrate Hbs, HMP reactivity has been analysed towards the typical ligands, that are imidazole for the ferric heme iron and CO and O_2 for the ferrous heme iron.

3.4.1 Heme-iron ligand binding properties of ferric HMP

In the present investigation, the imidazole binding properties have been studied in detail since this ligand displays binding and release kinetics (see below) that are fast enough to allow for accurate equilibrium titrations even at very low (< 10^{-5} M) ligand concentrations. Titration experiments of ferric HMP with imidazole yielded different results when performed with lipid free or UFA, CFA or TLE saturated protein. Titration profiles of lipid bound HMP were fitted to the simple, one binding site, reaction Scheme I (Fig. 16). Imidazole equilibrium binding curves of lipid free HMP were fitted to the reaction Scheme II.

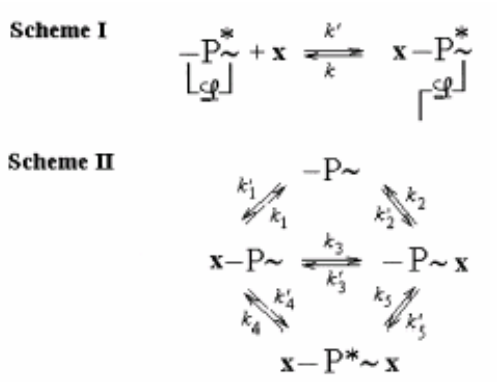

Fig. 16 Reaction schemes for ligand binding to ferric *E. coli* flavohemoglobin.
Ferric HMP has been inferred to possess a heme iron ligand binding site (-P) and a non heme binding site (P~). Both sites are involved in the recognition of lipid (UFA or CFA) substrates ( ). The interaction of the lipid with the heme site is weak and can be diplaced by heme iron ligands (x), as depicted in Scheme I. Complete removal of the bound lipid renders the non-heme site available for ligand interaction as outlined in Scheme II. Ligand binding to the heme iron and is accompanied by a fast ligand exchange (k_3 and k_{-3}) between the heme and the non-heme binding sites. Full saturation of both sites implies a conformational transition from P to P* species.

The presence of two ligand binding sites in Scheme II may appear paradoxical in a monomeric hemoprotein. Nevertheless, the presence of a single difference spectrum upon ligand binding (see Fig. 17) together with the strongly biphasic titration profile (Fig. 18) suggest an unusual mechanism of ligand saturation. The binding polinomial obtained from Scheme II is:

$$Y = \frac{[x\text{-}P\sim] + [\text{-}P\sim x] + [x\text{-}P^*\sim x]^2}{2\,C_{tot}} = \frac{K_1 x + K_2 x + K_4 K_1 x^2}{2\,\{1 + K_1 x + K_2 x + K_4 K_1 x^2\}} \quad ; \qquad eq.\ (1$$

Where x-P~ represents the protein with heme bound imidazole, -P~x is the protein with imidazole bound in the non-heme site and x-P*~x is the doubly ligated species in which both the heme and non-heme site are occupied by the imidazole ligand. It is important to point out that the biphasic imidazole titration profiles cannot be corrected for the contribution of species spectrally different from that of unliganded and fully liganded derivatives. In other words, all spectra obtained within the imidazole titration experiments are accounted for a linear combination of the unliganded derivative and of the fully ligated adduct. The observed biphasic titration profiles can be fully described in terms of the Scheme II of Fig. 16 under the

assumption that imidazole binding to the non-heme site is spectroscopically silent. Hence the species -P~x does not contribute to the observed signal and the species x-P*~x yields the same spectral contribution as x-P~ and the observed signal was fitted to a modified binding polynomial:

$$Y_{obs} = \frac{[x\text{-}P\sim] + [x\text{-}P^{*}\sim x]}{C_{tot}} = \frac{K_1 x + K_4 K_1 x^2}{1 + K_1 x + K_2 x + K_4 K_1 x^2} \quad ; \qquad \textit{eq.}\ (2$$

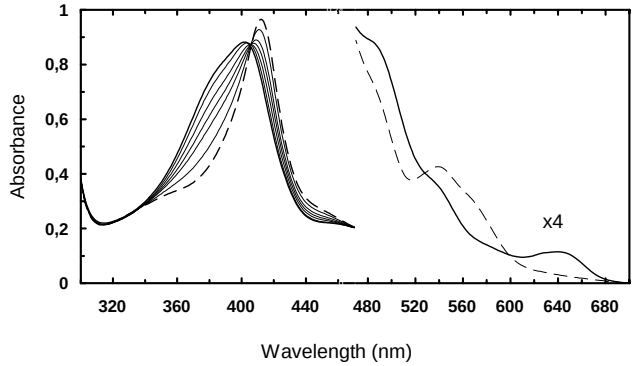

Fig. 17 Spectrophotometric titration of ferric *Escherichia coli* flavohemoglobin with imidazole.
Spectral changes accompanying the titration of the ferric protein with imidazole are shown in the visible (right) and Soret (left) regions. The spectrum of the unliganded derivative is rendered as a solid line whereas the dashed line pertains to the imidazole saturated spectrum.

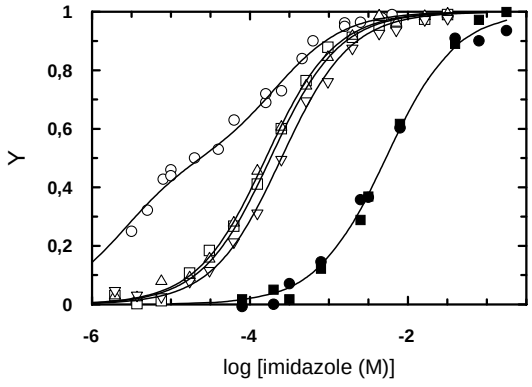

Fig. 18 Ligand binding isotherms of ferric *E. coli* flavohemoglobin and *horse* Mb with imidazole.
Titration experiments were carried out with imidazole on the lipid free HMP (O) and on HMP saturated with palmitoleic (□), cyclopropan-palmitoleic (Δ) and total *E. coli* lipid extracts (∇) in 0.1 M phosphate buffer at pH 7.0 and 20 °C. Control experiments have been also carried out on horse Mb in the presence (■) and in the absence (●) of TLE. Continuous lines represent fitting curves obtained by minimizing the experimental data to the schemes I and II (see Fig. 16 and Table I). The apparent equilibrium constant for imidazole binding to the protein saturated with palmitoleic, cyclopropan-palmitoleic and total *E. coli* lipid extracts were 1.8±0.5, 2.5±0.7 and 3.6±0.2×10^3 M^{-1} respectively.

As shown in Fig. 18, a simple single site titration profile is observed in the case of UFA (or CFA and TLE) saturated protein whereas lipid free protein displays a strongly biphasic behaviour characterized by a high affinity site (C½ around 1×10^{-5} M) and a low

affinity one (C½ around 1×10^{-3} M). The overall affinity of lipid saturated protein for imidazole is drastically decreased with respect to the high affinity site in the lipid free protein and is centred around 3×10^{3} M^{-1}. Fitting the equilibrium data with the binding polynomial given in *eq.* 2 yielded a complete set of thermodynamic constants whose values are reported in Table I. Such a minimal reaction scheme imposes severe constraints on the values of the equilibrium constants. In particular, the value of K_3 appears to be frozen around unity as it determines the amplitudes of the two phases and thus the flexus in the titration profile. As a consequence, $K_1 \approx K_2$ and $K_4 \approx K_5$ thus implying that the intrinsic affinity of the ligand molecule for the heme site and for the non-heme site is very similar. In Fig. 18, control experiment performed on horse Mb are also shown. These data indicate that the imidazole titration profile of the protein is unaffected by the presence of TLE (ten molar excess of lipids with respect to the protein).

The kinetic behaviour of imidazole binding to HMP has been thoroughly analyzed in rapid mixing experiments. Imidazole binding kinetics of lipid bound (TLE) HMP is accounted for a simple second order process with a rate constant of 8×10^{4} $M^{-1}s^{-1}$ (see Fig. 19, panel B). The rate of imidazole release calculated from the ratio between the second order rate and the equilibrium constants (3.6×10^{3} M^{-1}) is 22 s^{-1} whereas the same constant obtained from the pseudo first order plot (intercept with the Y axis) is around 6 s^{-1}. The origin of such a discrepancy has not been understood. Imidazole combination reaction of lipid free HMP (Fig. 19, panels A and B) also proceeded as an apparent single second order process under ligand concentration range that covered full saturation of the high affinity site and partial saturation of the low affinity site. The measured apparent combination rate was 4-5 faster than in lipid bound HMP yielding a value of 4×10^{5} $M^{-1}s^{-1}$, as estimated from the pseudofirst order plot of Fig.19 panel B. The rate of imidazole release in the pseudofirst order plot of Fig. 19 B seems to converge to about the same value as in the lipid bound protein. Obviously, it cannot be compared with the value(s) calculated from the equilibrium constants and the second order rate constant. Thus, the whole set of imidazole binding time courses, measured on the lipid free protein, have also been fitted explicitly to Scheme II by imposing the value of the equilibrium constants obtained from the fitting of the titration data. The values of the rate constants obtained from the global fitting procedure are given in Table I. Cyanide combination kinetics was also measured in both lipid free and lipid bound HMP (data not shown). Time courses were characterized by a second order rate constant of 1.2×10^{2} M^{-1} s^{-1} indicating that cyanide binding kinetics is insensitive to the presence of the bound lipid.

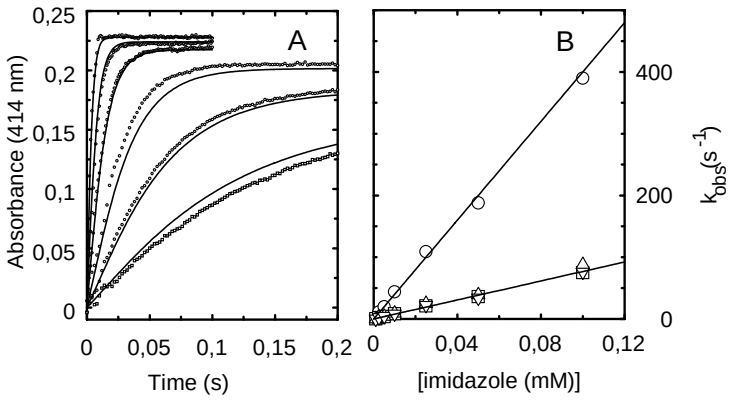

Fig. 19 Imidazole combination kinetics to ferric *E. coli* flavohemoglobin.
Panel A: imidazole combination time courses to ferric, lipid free HMP. Imidazole concentrations are reported in the abscissa of panel B. Continuous lines are the result of a global fitting procedure to Scheme II. The rate constants obtained are listed in TableI.

Panel B: Apparent pseudo first order rates of the time courses reported in panel A as a function of imidazole concentration. Continuous lines represent linear fits to the data and yield apparent second order rate constants of $4.1\pm0.1\times10^5$ M^{-1} s^{-1} for imidazole binding to the lipid free protein and of $8.5\pm0.2\times10^4$ M^{-1} s^{-1} for imidazole binding to HMP complexed with palmitoleic (□), ciclopropan palmitoleic (Δ) and TLE (total *E. coli* lipid extracts) (∇), respectively. Experiments were carried out in 0.1 M phosphate buffer, pH 7.0 and 20 °C. Protein concentration was 3-4 μM (after mixing).

Equilibrium constants		*Rate constants*	*(s^{-1})*
K_1	$2.0\pm0.15\times10^5$ M^{-1}	k_1	22
K_2	$2.2\pm0.25\times10^5$ M^{-1}	k_2	0.3
K_3	1.1	k_3	> 1000
K_4	$6.6\pm0.3\times10^3$ M^{-1}	k_4	0.05
K_5	6.0×10^3 M^{-1}	k_5	4

Table I: Summary of thermodynamic and kinetic parameters for imidazole binding to ferric, lipid free, *E. coli* flavohemoglobin.

The equilibrium constants for imidazole binding to HMP were obtained by fitting the data of Fig. 17 to the binding polynomial relative to the reaction Scheme II (*eq*. 2). The rate constants were obtained according to the global fitting procedure of the data shown in Fig. 18, panel A to the reaction Scheme II (Fig. 16). In the data fitting of the rate constants, the equilibrium constants K_1 to K_5 were fixed and the first order rates of ligand release were allowed to float. Thus, the combination rate constants (k_1', k_2', k_4' and k_5') can be obtained from the equilibrium constants and the dissociation rate constants. The values of the ligand release constants are devoid of standard deviations as they are the result of a global fitting procedure. K_2 and K_4 values are automatically determined according to Scheme II.

3.4.2 Heme-iron ligand binding properties of ferrous HMP

The ligand binding kinetic properties of the ferrous protein have been investigated by measuring the second order binding rates of CO and the first order kinetics of oxygen release on both the lipid free protein and on HMP saturated with different lipids or fatty acids. Lipid free HMP yielded biphasic second order CO binding kinetics whose rates and amplitudes (k_1 = 1.8×10^7 $M^{-1}s^{-1}$ (68 %) and k_2 = 1.2×10^6 $M^{-1}s^{-1}$ (32%)) were almost superimposable to those obtained by Gardner et al. (2000). In contrast, experiments carried out on the protein saturated with TLE yielded perfectly monophasic CO ligand rebinding time courses after photolysis with a second order rate of 5.1×10^6 $M^{-1}s^{-1}$ (Fig. 20). In Fig. 20, the time course of CO rebinding after photolysis are shown in semilogarithmic plots. The absorbance decreases at 434 nm are the results of three linear records obtained in the nanosecond to millisecond time regime. In both lipid free and lipid saturated protein, no geminate recombination processes were detected as demonstrated by the flatness of the nanosecond time recording. CO release kinetics were not measured due to the difficulty in obtaining unbiased time courses with the NO displacement method in the presence of a concomitant NO reduction (to N_2O) reaction.

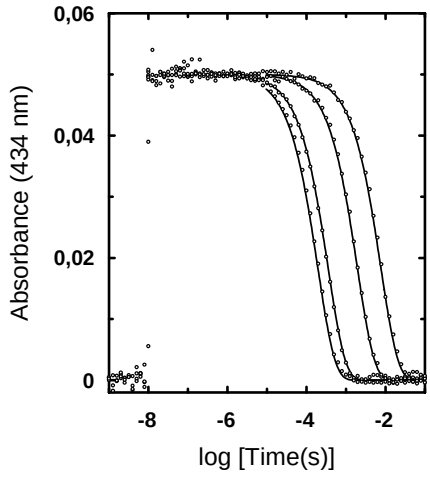

Fig. 20 Kinetics of CO binding to ferrous *E. coli* flavohemoglobin.
Time courses of CO recombination after photolysis of TLE treated HMP as a function of CO concentration. The experiment has been carried out in 0.1 M phosphate buffer at pH 7.0 containing 250 μM NADH and 1 mM EDTA at 20 °C. Continuous lines represent monoexponential fits to the experimental points that yield a second order rate constant of $5.1\pm1.1\times10^6$ $M^{-1}s^{-1}$. The points in each data set (12000 points merged from three different acquisitions in the nanosecond, microsecond and millisecond time regime) have been logarithmically sampled.

The kinetics of oxygen release, as monitored in oxygen pulse experiments (Fig. 21), are likewise biphasic in lipid free HMP with first order rates (k_{off}) of 2.2 s^{-1} (44%) and 0.11 s^{-1} (56%), respectively. In contrast, oxygen release from the TLE saturated protein are accounted for by a single exponential decay (k_{off} = 0.16 s^{-1} at 20 °C). The behaviour of O_2 release kinetics in HMP saturated with palmitoleic and cyclopropan-palmitoleic acid is intermediate between the lipid free and TLE saturated HMP in that the amplitude of the fast phase is decreased but not abolished. Direct oxygen binding kinetics have not been reported. Laser photolysis experiments on the oxygenated derivative are in fact severely biased by the NADH driven oxygen consumption occurring during the experiments thus requiring a more complex flow-flash measurements.

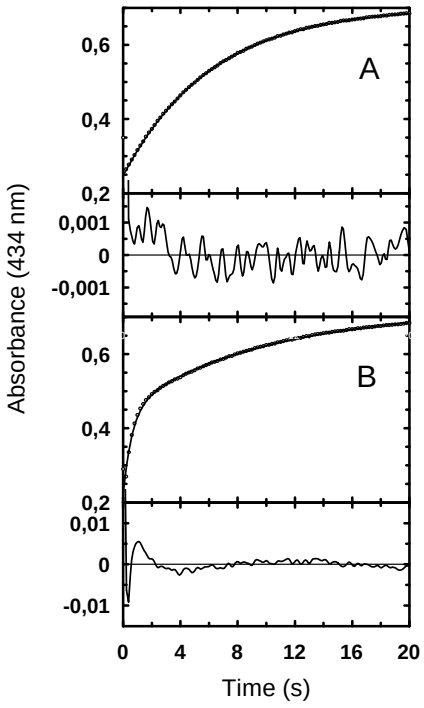

Fig. 21 Kinetics of oxygen release in ferrous *E. coli* flavohemoglobin.
Time courses of oxygen release from TLE treated and lipid free HMP (panels A and B, respectively) have been obtained in oxygen pulse experiments (see Materials and Methods). Data in panel A have been fitted to a single exponential decay with an apparent rate of 0.16±0.01 s^{-1}. The kinetic record in panel B has been fitted to two exponentials characterized by apparent first order rates of 2.2±0.2 s^{-1} (44%) and 0.11±0.03 s^{-1} (56%), respectively. The experiments have been carried out in 0.2 M phosphate buffer at pH 7.0 containing 25 mM sodium dithionite (after mixing) at 20 °C.

3.4.3 Ligand binding properties of the mutant GluH23-Val

In order to value the effect of the hydrogen bonding network involving the proximal histidine, oxygen release and carbon monoxide binding were measured on a HMP mutant in which GluH23 is substituted by valine.

Interestingly, the affinity of the mutant for the phospholipid was increased with respect to the native protein such that the bound lipid could not be removed without denaturing the protein. Thus, ligand binding experiments have been carried out on the lipid bound derivative only. The oxygen release monitored in the oxygen pulse experiment shows a single exponential decay at 436 nm with a $k_{off} = 24\ s^{-1}$ at 20 °C (Fig. 22), that is two order of magnitude higher than that observed for the native protein.

The CO binding, instead, is apparently unaffected by the mutation and is comparable with the data obtained for lipid bound HMP.

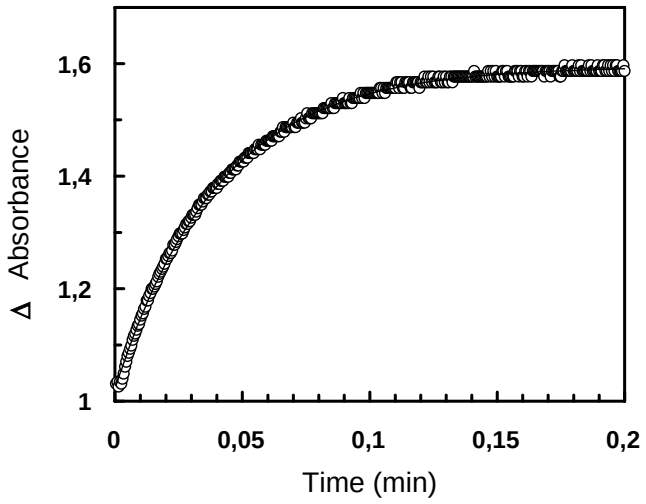

Fig. 22 Kinetics of oxygen release in HMP Glu H23-Val.
The time course of oxygen release has been only measured for the lipid bound protein as the affinity for this ligand is higher in the mutant than in the native protein. Removing the phospholipids is not feasible without destroying the protein. The kinetic is monophasic and shows a k_{off} of 24 s^{-1} at 20°C and in the presence of 0.2 M phosphate buffer at pH 7.0 containing 25 mM sodium dithionite.

3.5 ENZYMATIC ACTIVITY

The observed specificity for UFA and CFA binding within the active site of HMP strongly suggested a possible enzymatic activity towards these fatty acids. In particular, it was postulated that HMP might be endowed with a peroxidase or p450-like activity towards unsaturated phospholipid substrates possibly yielding oxygenated adducts on the double bond. Mono/dioxygenation and/or hydroxylation reactions were screened on several UFAs and CFAs as well as on aromatic hydrocarbons (benzene, toluene, naphthalene), and linear and cyclic alkenes (1-dodecene, 6-dodecene, cyclohexene, cyclooctene) by means of mass spectrometric analysis. The putative substrates were incubated in the presence of NADH, oxygen and variable amounts of protein. In spite of the high affinity for both oxygen and UFAs or CFAs and of the possibly favourable stereochemistry for oxygen addition to the acyl chain, no modifications of the fatty acid were detected under the experimental conditions used (i.e. pH 7.0, 20 °C and NADH as a reductant, see Table II).

Lipid type MW(g×mol^{-1})	*UV-Vis spectral changes*	*ESI mass*
L-α dipalmitoyl phosphatidyl choline	−	
L-α dipalmitoyl phosphatidyl ethanolamine	−	
L-α dipalmitoyl phosphatidyc acid	−	
palmitic acid	−	
stearic acid	−	
oleic acid	+	282 (282.5)*
palmitoleic acid	+	254 (254.4)
linoleic acid	+	278 (278.2)
cis vaccenic acid	+	282 (282.5)
9,10 methylen palmitoleic	+	265 (265.2)
aromatic hydrocarbons (benzene, toluene, naftalene)	−	
linear and cyclic alkenes (1 dodecene, 6 dodecene, cyclohexene, cyclooctene)	−	

* Number in parenthesis indicate the calculated monoisotopic molecular weigth.

Table II: Phospholipids and fatty acids binding to *E. coli* flavohemoglobin as screened by UV-Vis spectroscopy and ESI mass spectrometry.

HMP is instead able to reduce oxygen in the presence of NADH producing H_2O_2. This reaction could be due to an uncoupled cycle which happens in absence of the substrate. It has been observed in cytochrome p450 that the electron equivalents that are not utilized to oxidize substrate are liberated from intermediate steps of the reaction cycle in the form of hydrogen peroxide (Loida et al. 1993). Nevertheless, no substrate modification was observed in HMP in the presence of the putative lipid substrate. In contrast, HMP was able to efficiently reduce hydrogen peroxide to water at the expenses of NADH reducing equivalents and under low oxygen content. This activity differs from the classical catalase activity (H_2O_2 disproportionation to yield water and molecular oxygen) in that entails hydrogen peroxide reduction to water without oxygen production. This enzymatic activity has been formerly defined as peroxide-reductase activity and is typical of a class of enzymes identified as peroxiredoxins (Nishiyama et al. 2001, Takeda et al. 2004). In turn, the peroxiredoxin family comprises enzymes that are also capable of reducing alkyl hydroperoxides, the alkyl hydroperoxide reductases (Hillas et al. 2000, Gaber et al. 2001, Fisher et al. 1999, Seaver et al. 2001). Thus, the peroxide and alkyl hydroperoxide reductase activity of HMP was investigated further.

Ferrous HMP has been demonstrated to posses a genuine alkyl hydroperoxide reductase activity in anaerobiosis, thus suggesting that HMP itself and possibly other member of the haemoglobin-like protein family are involved in the reduction of lipid membrane hydroperoxides.

The hydroperoxide reductase activity of HMP was screened by using H_2O_2, tert-butyl hydroperoxide, cumyl hydroperoxide and linoleic acid hydroperoxide as substrates. The reaction products, analyzed by HPLC, GC or ESI mass spectrometry revealed transformation of the alkyl hydroperoxide species into their corresponding alcohols. A complete, quantitative analysis of the reaction products carried out for cumyl hydroperoxide is shown in Fig. 23.

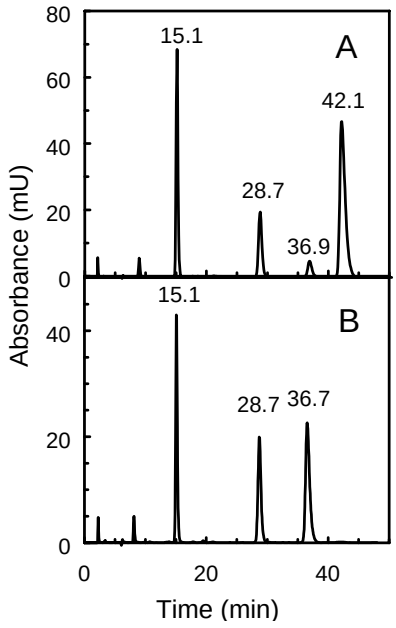

Fig. 23 HPLC elution profiles of the reaction products obtained from the reaction of *Escherichia coli* flavohemoglobin and cumyl hydroperoxide.

HPLC elution profiles of the reaction products obtained from the reaction of *Escherichia coli* flavohemoglobin and cumyl hydroperoxide.

Panel A represents the elution profile (at 256 nm) of a reaction blank obtained from ethyl acetate extraction of a solution containing NADH (5 mM) and cumyl hydroperoxide (2 mM) in 0.1 M phosphate buffer and pH 7.0 containing 1 mM EDTA (reaction carried out under N_2 atmosphere, 1 h incubation at 20 °C). Panel B represents the elution profile obtained from the same reaction mixture in the presence of 10 μM HMP. The peaks are assigned as follows: 42.1 min, cumyl hydroperoxide; 36.9 min (A) or 36.7 min (B), cumyl alcohol; 28.7 min, acetophenone; 15.1 min, benzyl alcohol (internal standard). Acetophenone is present as a contaminant in the stock solution (3%) and is recovered in a similar amount in both reaction mixtures of panels A and B. Note that the molar absorptivity of acetophenone at 256 nm is 30 fold higher than that of cumyl alcohol.

The ethyl acetate extracts obtained from the reaction mixture in the absence (blank) and in the presence of HMP, respectively, were analyzed by HPLC. Elution profiles are shown in panel A (blank) and Panel B. Benzyl alcohol (peak at 15.1 min) was used as an internal standard to quantify the reaction products. The elution profile of the blank in panel A demonstrates that stock solutions of cumyl hydroperoxide (peak at 42.1 min, 89 %) contained both acetophenone (peak at 28.7 min, 3% in) and cumyl alcohol (peak at 36.7 min, 8%) as contaminants. Data shown in panel B indicate a complete transformation of cumyl hydroperoxide into cumyl alcohol (peak 36.7 min) whereas the peak at 28.7 min reflects the small amount of acetophenone (whose molar absorptivity at 256 nm is about 30 fold higher with respect to that of cumyl alcohol) already present in the blank. Accordingly, GC mass data, performed in order to take into account the possible formation of other volatile reaction products, revealed full conversion of cumyl hydroperoxide into cumyl alcohol in the reaction mixture (data not shown).

ESI mass spectrometric data (Fig. 24) revealed a similar trend in the case of linoleic acid hydroperoxide. Mass spectra of the ethyl acetate extracts of the blank solutions (in which either protein or NADH were absent) yielded a major peak at 311 a.m.u. (corresponding to the molecular weight of linoleic acid hydroperoxide anion) whereas the dominant feature was at 295 a.m.u. (-16 a.m.u. with respect to the 311 peak) in the reaction mixture containing both protein and NADH. Spurious peaks at 334 and 317 a.m.u. (+22 with respect to 311 and 295 a.m.u., respectively, attributed to Na^+ ion adducts) are apparent in the blank and in the complete reaction mixture, respectively.

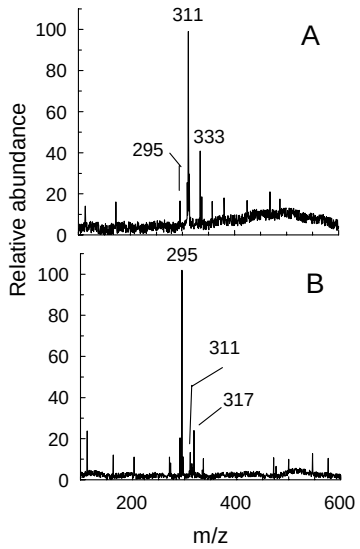

Fig. 24 ESI-MS spectra of the reaction products obtained from the reaction of *Escherichia coli* flavohemoglobin and linoleic acid hydroperoxide.
The spectrum of a reaction blank obtained from an ethyl acetate extraction of a solution containing NADH (0.5 mM) and linoleic acid hydroperoxide (140 μM) is shown in panel A. The major peak at 311 a.m.u. corresponds to linoleic hydroperoxide anion. Panel B represents the spectrum obtained from the same reaction mixture in the presence of 2 μM HMP. The major peak at 295 a.m.u. corresponds to linoleic alcohol. Experiments were carried out in 0.1 M phosphate buffer and pH 7.0 containing 1 mM EDTA (reaction carried out under N_2 atmosphere, 15 min incubation at 20 °C).

Reaction kinetics were monitored on the different substrates by means of UV-visible absorption spectroscopy in both spectrophotometric experiments at low protein concentrations (0.2-1 μM) and in stopped flow, rapid kinetic measurements at higher protein concentrations (4-6 μM). HMP activities, determined upon increasing amounts of alkyl hydroperoxides or H_2O_2 to degassed HMP solutions in the presence of excess NADH (250 μM) are depicted in Fig. 25. Double reciprocal plots of Fig. 25 are the result of several separate experiments carried out on different protein preparations.

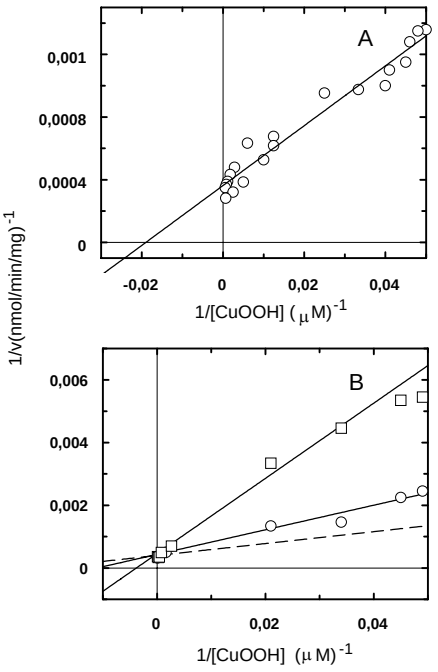

Fig. 25 Double reciprocal plots of *Escherichia coli* flavohemoglobin alkylhydroperoxide reductase activity versus cumyl hydroperoxide concentrations.
The activities were measured under N_2 atmosphere in the presence of 0.2-1 μM protein, 250 μM ΝΑΔΗ ιν 0.1 Μ πηοσπηατε β υφφερ ατ πΗ 7.0. Τηε στραιγητ λι νε ρεπρεσεντσ α λινεαρ φιττινγ τ ο τηε εξπεριμενταλ δατα. Ιν πανε λ Β, ΧΟ ινηιβιτιον οφ τηε αλκψλ ηψδροπεροξιδε ρεδυχτασε αχτιω ιτψ ωερσυσ χυμψλ ηψδροπεροξι δε ισ σηοων. Τηε δασηεδ λινε χο ρρεσπονδσ το τηε λινεαρ φιτ ρεπ ορτεδ ιν πανελ Α. Τηε χοντινυου σ λινεσ ρεπρεσεντ τηε λινεαρ φιτ σ το τηε δατα οβταινεδ ιν τηε σα

Data linearization and fitting yielded the set of steady state kinetic parameters reported in Table III. The highest activity was observed for cumyl and linoleic acid hydroperoxides whereas reduction of tert-butyl hydroperoxide and hydrogen peroxide was two- and three-fold slower, respectively (Table III). It should be pointed out that reaction with linoleic acid hydroperoxide is strongly solvent dependent. Data obtained in the presence of 0.1% Triton X–100 were fully reproducible and displayed nearly zeroth order kinetics. In contrast, experiments carried out in 20 % ethanol/water mixture (in which substrate is soluble up to 2-3 mM concentration at 25 °C) exhibited a slightly slower rate and displayed nearly exponential time courses.

hydroperoxide	K_m (μM)	V_{max} (nmol/min/mg)*
H_2O_2	260±28	789±102
Tert-Butyl	76±15	1125±135
Cumyl	55±15	2564±155
Linoleic	26±14[a]	1876±188[a]
	115±33[b]	872±215[b]

[a] 0.1% Triton X-100

[b] 20% etanol/water mixture

* For comparison with data from other authors, activities can be redimensioned "per mol" using the molecular mass of 43,000 g mol^{-1} for HMP.

Table III: *Escherichia coli* flavohemoglobin steady state kinetic constants for hydroperoxide substrates. Data were obtained in 0.1 M phosphate buffer pH 7.0 containing 250 μM NADH, 1mM EDTA and 25 °C. a) 0.1% Triton X-100; b) 20% ethanol/water mixture.

Carbon monoxide inhibition of the hydroperoxide reduction reaction was also determined for cumyl hydroperoxide. The data reported in Fig. 25 B indicate a clear competitive inhibition mechanism by CO with an apparent Ki of about 0.2 μM (calculated from the apparent K_m^{app} values according to a simple Michelis Menten formalism).

Rapid kinetic experiments, carried out by mixing degassed HMP solutions (8 μM) in the presence of excess NADH (320 μM) with cumyl hydroperoxide (1 mM) solutions are depicted in Fig. 26 A. The kinetic spectral profiles were characterized by a fast decay at 340 nm (t1/2 = 3 s) due to NADH oxidation while HMP remains in its fully reduced (ferrous heme, reduced flavin), deoxygenated derivative. Upon depletion of NADH reducing equivalents (5-6 s), HMP undergoes complete oxidation (ferric heme, oxidized flavin). A similar trend is observed with linoleic acid hydroperoxide whereas the formation of a spectroscopically distinct contribution characterized by a an absorption peak at 420 nm was noticed under stationary state conditions in the reaction with tert-butyl hydroperoxide (data not shown). The species characterized by the 420 nm peak was the dominant feature in the reaction of ferrous HMP with hydrogen peroxide (Fig. 26 B). Analysis of the time dependent spectral profiles of Fig. 26 allowed the identification of the absorption spectra relative to each species (see also Fig. 27). The spectral profile 3 obtained from the data of Fig. 26, was thus attributed to an oxo-ferryl heme iron adduct by analogy with the spectra of typical Compounds II of peroxidases and must be distinguished from the ferrous heme iron dioxygen adduct (profile 4). The oxo-ferryl adduct was relatively stable (seconds to minutes) under reducing conditions (250 μM NADH) and 50-250 μM hydrogen peroxide concentrations whereas it rapidly decayed to a mixture of ferric heme and unidentified heme degradation

products in the presence of H_2O_2 in larger excess (> 2 mM). In order to confirm the oxo-ferryl spectrum assignment, the following set of controls were carried out: i) the species obtained in the presence of H_2O_2 and NADH was mixed with CO saturated solutions (1 mM) in a double mixing experiment and no spectral changes were observed; ii) the same compound could not be reduced with sodium dithionite.

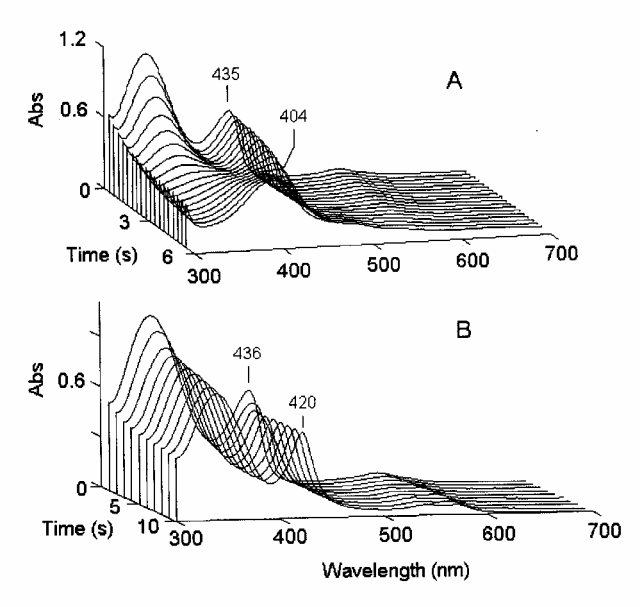

Fig. 26 UV-Visible absorption spectral changes accompanying hydroperoxide reductase activity in *Escherichia coli* flavohemoglobin.
Spectra were collected with a diode array device after mixing a solution of ferrous HMP (8 μM) containing 250 μM NADH with a solution containing 1 mM cumyl hydroperoxide (A) or 1 mM H_2O_2 (B). The measurement has been carried out in 0.1 M phosphate buffer at pH 7.0 containing 1 mM EDTA and 20 °C. Solutions were degassed and kept under nitrogen before use.

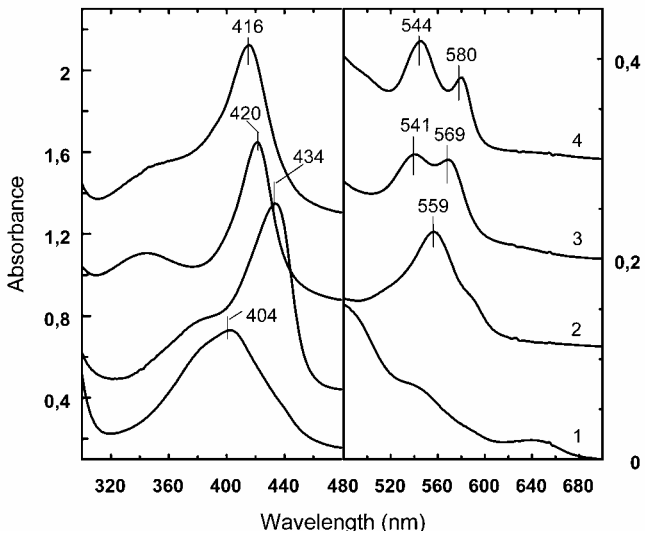

Fig. 27 UV-Visible absorption spectra of *Escherichia coli* flavohemoglobin intermediates in its reaction with alkyl hydroperoxides.
The spectrum of ferric HMP (1) has been taken at the end (10 s) of the reaction of HMP with cumyl hydroperoxide. NADH reduced, deoxygenated HMP spectrum (2) was collected before mixing with cumyl hydroperoxide. The spectrum of the HMP Compound II intermediate (3), obtained as a transient species from the experiment carried out with H_2O_2 (see Fig. 3, Panel B), can be compared with the spectrum of fully reduced, dioxygen HMP adduct (4). Spectra 2, 3 and 4 have been corrected by subtracting the contribution of NADH. All spectra have been taken at pH 7.0 in 0.1 M phosphate buffer.

This data suggest that HMP is capable of recognizing the alkyl hydroperoxide moiety because of the highly hydrophobic distal heme pocket, and in the case of peroxidized phospholipids containing unsaturated fatty acids, HMP is able to adjust the hydrocarbon chain kink in correspondence of the cis double bound above the heme iron. The binding of the hydroperoxide to the ferrous heme iron occurs with the concomitant two electron reduction and the cleavage of the dioxygen bond and consequent formation of a peroxidase-like Compound II and an alkyl alcohol (see Fig. 28).

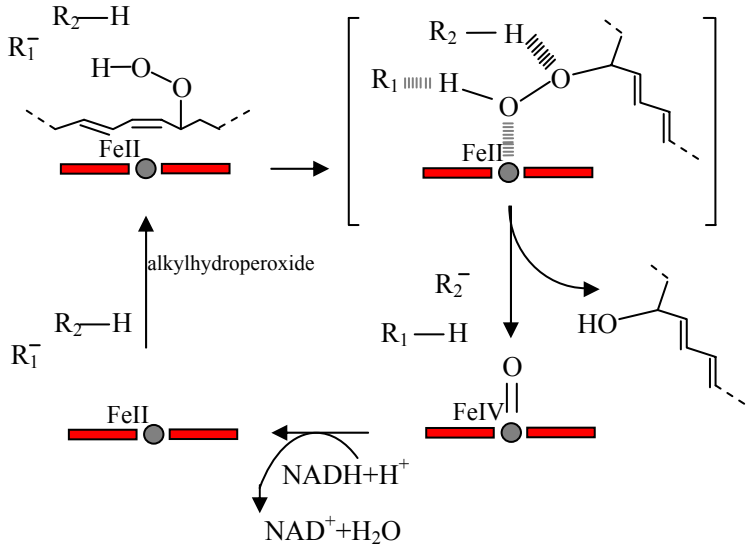

Fig. 28 Probable reaction scheme catalyzed by HMP.
The ferrous protein is able to bind the hydroperoxy-phospholipid by recognizing the double bond. The hydroperoxide is reduced to alcohol and the heme-iron is oxidized to Compaund II. Reduction of the oxo-ferryl compound to water and ferric heme with concomitant flavin oxidation and release of the hydroxy-phospholipid to the membrane may be hypothesized. R1 and R2 represent two not yet identified species (protein's aminoacids or water molecules) that are able to exchange protons.

4. DISCUSSION

The results obtained in the present thesis have brought out a complete picture of *Escherichia coli* flavohemoglobin structure and of its functional properties in vitro. The solution of the tridimensional structure, the analysis of the ligand binding properties, the identification of a putative physiological function and the comparative analysis of the sequences of the flavohemoglobin family have been carried out and will be discussed also in the light of other most recent publications in the field.

4.1 THE TRIDIMENSIONAL STRUCTURE OF HMP

The structure of flavohemoglobins represents a paradigmatic example among multidomain proteins in which two modules with different functions are fused together in order to create a protein endowed with entirely novel functional properties. The first tridimensional structure of a flavohemoglobin, obtained in 1995 by Ermler et al. (*Alcaligenes eutrophus* flavohemoglobin, FHP), had shown that flavohemoglobins are made of a C-terminal NAD- FAD-binding domain, member of the FdR-like family, and an N-terminal globin domain (Fig. 1). Surprisingly, inspection of the structure of the globin domain active site in FHP revealed that the distal heme pocket was occupied by a phospholipid molecule. The presence of this bulky ligand was apparently unrelated to possible functional roles of FHP and rendered the understanding of the geometry of the active site particularly difficult. On this basis, the first part of the present work was devoted to the crystallization of the highly homologous *Escherichia coli* flavohemoglobin in its lipid free form. The overall structure of ferric unliganded HMP, obtained at 1.6 Å resolution, brings about analogies and differences with the structure of the globin domain of the flavohemoglobin from *Alcaligenes eutrophus* and of the highly similar single chain hemoglobin from *Vitreoscilla sp* (Tarricone et al. 1997, Bolognesi et al. 1999).

The globin domain is structurally analogous to vertebrate myoglobins. It consists of eight alpha helices (A, B, C, …H) that enclose the heme cofactor within a hydrophobic pocket in which the heme iron is coordinated by His F8 on the proximal side. Inspection of the distal heme pocket in HMP (ferric unliganded derivative) has brought out a very different picture from that initially proposed on the basis of the tridimensional structures of FHP (ferrous derivative in the presence of a phospholipid) and VHB (ferric cyano-met, aquo-met and azido-met) derivatives. In fact, in HMP, the distal side is occupied by the Leu E11 isopropyl side chain that shields the heme iron from the residues in the topological positions predicted to interact with heme iron bound ligands, namely Tyr B10 and Glu E7, and stabilizes a pentacoordinate ferric iron species. This unique architecture, completed by the canonical Phe CD1 residue, provides a very hydrophobic shell on the top of the iron atom such that displacement of the Leu E11 side chain is necessary in order to allow ligand binding to the iron atom. Thus, Leu E11, can be considered as the genuine distal residue in flavohemoglobins in the same manner as His E7 is the canonical distal residue in most vertebrate hemoglobins. In this frawework, it is of interest to comment on the differences observed between the ferric unliganded HMP and the ferrous, phospholipid bound FHP.

The main differences between these two proteins are the E helix positioning within the globin domain and a rotation of the NAD-binding module. These structural changes must be attributed to the presence of the phospholipid molecule in FHP. Thus, the comparison between ligand free HMP and ligand bound FHP is strongly suggestive of a ligand linked conformational change that entails the rotation of the Leu E11 isopropyl side chain (accompanying the movement of the E helix) towards the edge of the heme in order to allow the Tyr B10 phenol hydroxyl interact with the iron bound ligand. This interpretation explains the experimental evidence obtained by resonance Raman and FTIR spectroscopy, for the participation of a Tyr hydroxyl (either direct or most likely mediated by a water molecule) to the distal coordination of bound CO in the ferrous protein (Mukai et al. 2001, Bonamore et al.

2001). In fact, previous Raman and FTIR measurement showed that ferrous CO-bound HMP is characterized by the presence of two conformers in which the diatomic ligand is either stabilized by a hydrogen-bonding interaction to the Tyr B10 (closed conformation) or free of distal constrains (open conformation). The present structure pertaining to a ligand free derivative offers a different view in which the Tyr B10 residue lies far from the diatomic ligand contact region and is shielded by the isopropyl side chain of Leu E11. Thus, the positioning of Leu E11 indicates that this residue not only gates the accommodation of the incoming ligand but also hinders the access of the Tyr B10 phenol hydroxyl to the distal ligand contact area. In other words, a ligand linked motion entails the displacement of the Leu E11 side chain (open conformation) followed by the approaching of the Tyr B10 hydroxyl to the iron-bound ligand to form a hydrogen bonding interaction (closed conformation).

The proximal heme environment in flavohemoglobins is also peculiar and differs from that observed in vertebrate hemoglobins and myoglobins in that the proximal histidine is involved in a hydrogen bond network with Glu135 and Tyr95 (Fig. 3). These observations, coupled to resonance Raman data (Mukai et al. 2001), indicate that HMP as well as FHP and in general bacterial hemoglobins bear more resemblance to peroxidases rather than hemoglobins. In fact the Tyr B10-Gln E7 pair may play a similar role as the distal His-Arg pair in peroxidases and the proximal histidine is involved in a strong hydrogen bond interaction with a carboxyl group (Asp235 in cytochrome c peroxidase, Glu135 in HMP).

Regarding the FAD-binding domain, the structural overlay of the isoalloxazine binding motif in lipid free HMP versus lipid bound FHP reveals a structural rearrangement of the C-terminal segment that face the NAD-binding side of the flavin ring. This structural change has been interpreted as a specific signature of a phospholipid induced conformational transition in FHP that also entails a movement of the whole NAD binding module with respect to the FAD-binding domain (Fig. 5).

The clarification of the structural properties of HMP with respect to FHP and the understanding of the architecture of the active sites of these proteins allowed a rational evaluation of the structure based alignments of the whole flavohemoglobin family. Sequence alignments were carried out on Gram negative bacteria (*Enterobacteriaceae*, *Vibrionaceae*, *Pseudomonaceae*, *Rhizobiaceae)* as well as on Gram positive bacteria (*Bacillaceae* and *Micrococcaceae)* and even unicellular eukaryotes. The flavohemoglobin family is formed by a very homogeneous group of proteins that share highly conserved active sites in both the heme and flavin binding domains. A multiple sequence alignment of about 50 proteins from different bacterial and eukaryotic microorganisms shows that the residues surrounding the heme cofactor in HMP, namely Tyr B10, Glu E7, Lue E11, His H8, Glu135, Tyr95 are conserved in all analyzed flavohemoglobins (Fig. 7A). The residues involved in the creation of a hydrophobic moiety for the phospholipid accommodation in FHP and that ones contouring the flavin binding cavity are also conserved (Fig. 7B).

The high similarity among all flavohemoglobins obviously suggests common functional properties. In particular, the presence of the tightly bound phospholipid within the heme pocket of *A. eutrophus* flavohemoglobin suggested the participation of bacterial hemoglobins to some sort of lipid membrane transport and/or processing (Ollesch et al. 1999). More recently, the single chain bacterial hemoglobin from *Vitreoscilla* sp. (VHB) and the truncated hemoglobin from *Mycobacterium tubercolosis* (HbO) have been reported to be preferentially located in contact with the bacterial inner membrane in vivo and to be capable of reversible binding to liposome obtained from bacterial lipid extracts in vitro (Ramandeep et al. 2001, Pathania et al. 2002). HMP itself has also been reported to interact with membrane phospholipids although with no apparent specificity for any kind of lipid molecule (Ollesch et al. 1999). The lipid binding properties of HMP have thus been investigated in detail.

4.2 LIGAND BINDING PROPERTIES

4.2.1 Lipid binding properties

The presence of a phospholipid within the heme pocket of the *Alcaligenes eutrophus* flavohemoglobin prompted the investigation of the lipid binding properties in HMP in order to determine whether lipid binding is a general property of flavohemoglobins and whether it may have a physiological significance. In simple UV-visible absorption experiments it was demonstrated that HMP is capable of interacting with bacterial lipid membranes and is also able to recognize specifically UFA and CFA. These data challenge previous reports on *Vitreoscilla* hemoglobin, *Alcaligenes eutrophus* flavohemoglobin and HMP itself that envisaged an unspecific interaction with membrane phospholipids (Ollesch et al. 1999, Ramandeep et al. 2001). Most interestingly, binding of UFA or CFA to HMP gives rise to a clear spectroscopic change in the visible spectrum of the ferric heme (Fig. 9). In fact, the absorption spectrum of the unliganded derivative corresponds to a typical pentacoordinated heme adduct in which the proximal histidine is the fifth ligand, as demonstrated by the peak at 645 nm and the broad Soret band, characterized by a low molar absorptivity and centered around 403 nm (Boffi et al. 1999). In contrast, the spectrum of the UFA (or CFA) saturated species displays a sharp peak at 407 nm and a shallower one at 625 nm and is very similar to that of high spin adducts observed in many other hemoglobins and myoglobins in the presence of weak ligands such as fluoride (Antonini et al. 1971, Giangiacomo et al. 2001). Thus, the spectral profile of lipid bound HMP is diagnostic of the formation of a hexacoordinated species in which the sixth coordination position is occupied by a component of the fatty acid chain. We propose that the double bound or cyclopropane ring recognition by the flavohemoglobin involves a weak but direct bonding interaction to the heme iron atom. Nevertheless, inspection of the crystal structure of the ferrous, lipid bound, *A. Eutropus* FHP (1.75 Å resolution) indicates that the iron-nearest carbon atom (CA of the cyclopropane ring, see Fig. 12) in ferrous, lipid bound, FHP is at 3.5 Å distance from the metal. Such distance preclude any bonding interaction between the iron atom and the distal ligand in that no orbital overlap can be predicted to occur involving the dz^2 ferrous or ferric iron orbital at a distance higher than 3.0 Å. Interestingly, the ferric, ligand free, HMP (1.6 Å resolution) displays similar structural features within the iron first coordination shell with the CG carbon atom of LeuE11 at 3.4 Å distance from the iron atom. Thus, in ferrous lipid bound and ferric lipid free flavohemoglobins, the iron atom preserves a pentacoordinate stereochemistry and establishes no bonding interactions at the distal site. Our results on the ferric lipid bound HMP complete the picture but also offer a different view. In agreement with the crystallographic data, optical absorption (both in solution and in the crystals) and resonance Raman spectroscopy points out unambiguously that the lipid free, ferric derivative is a pentacoordinate species and the LeuE11 residue does not establish a bonding interaction with the ferric iron. In contrast, the formation of a hexacoordinate derivative is clearly demonstrated upon lipid binding to the ferric HMP protein by the low frequency shift of the core size marker bands (Choi et al. 1982, Boffi et al. 1999). The appearance of a hexacoordinate high spin species is accompanied by an unusually intense band at 319 cm^{-1}, attributed to a γ_6 heme out of plane vibrational mode (Fig. 10). The conversion from a pentacoordinate to a hexacoordinate species is consistent with the formation of an axial bonding interaction between the ferric heme iron and the lipid (linoleic acid or TLE) moiety. Our analysis pointed out that lipid induced spectral changes, attributed to lipid binding, are specific for UFA and CFA free fatty acids as well as for negatively charged phospholipids esterified with a UFA or a CFA molecule. UFA or CFA methyl esters are not recognized by the protein binding site. No binding has been detected with saturated phosphatidil ethanolamine and phosphatidyl glycerol derivatives (the most abundant phospholipids within *E. coli* membrane) nor with saturated fatty acids and simple linear or cyclic hydrocarbons containing *cis* double bonds. Thus, on the basis of the structural data of Ollesch et al. (1999), an explicit model for UFA or CFA binding to HMP has been proposed

in which the negatively charged part of the lipid moiety is hosted in an anion binding cavity located next to the heme pocket and the cyclopropane ring or the double bond are directly coordinated to the iron atom. In order to single out the nature of such an unusual iron-ligand bonding interaction EXAFS measurements have been carried out in parallel on the ligand free and lipid bound protein. The picture that emerges from these studies is both enlightening and intriguing. Direct inspection of the FT spectra (Fig. 11, panel B) points out that differences between the lipid free and lipid bound ferric protein are manifest within a shell of 2-4 Å from the iron atom. In particular, when comparing the FT spectra of ligand free and lipid bound HMP, an additional shoulder 2.3 Å accompanied by an increase in intensity of the peak at 3.5 Å can be observed in the latter spectrum. This feature is assigned to an axial contribution in the sixth coordination position in lipid bound HMP. Quantitative analysis of the EXAFS data indicates that a bonding interaction does occur between the ferric heme iron and a couple of atoms located at 2.7 Å from the metal.

HMP Glu135-Val is also able to bind phospholipid with an even higher affinity than the native protein. In fact, the lipid is retained by the protein after the hydroxylapatite purification step, as well after a column of hydroxyalkoxypropyl-destrane, that removes phospholipids from native HMP.

Complete kinetic and thermodynamic parameters for fatty acid binding to ferric HMP have been obtained for linoleic acid only in the presence of ethanol (20 %) as a co-solvent. The binding constant, estimated from ligand binding and release data is about 4×10^7 M^{-1} (or k_d = 25 nM), a figure that is similar to that of true type fatty acid binding proteins (Balendiran et al. 2000).

The absence of binding to pure DPPC liposomes (DPPC is not synthesized in bacteria) indicates that HMP can actually recognize the polar heads of naturally occurring phospholipids of *E. coli* membrane and does not interact with the hydrophobic core of the bilayer. The identification of an anion binding site (fully compatible with a phosphate binding site) in a protein loop above the heme pocket allows one to hypothesize a recognition of the membrane through an interaction of the loop with the phosphate moiety of the phospolipid molecule. Thus, HMP most likely works at the interface between the cytosol and the bacterial inner membrane and is permanently saturated with a phospholipid esterified with either an UFA or a CFA molecule.

4.2.2 Heme-iron ligand binding properties of ferric HMP

The broad, biphasic equilibrium titration profile for ligand binding to ferric, lipid free HMP and VHB (Bolognesi et al. 1999) represents a puzzling thermodynamic behaviour that had not been understood as yet. In a previous investigation, ligand binding to VHB was interpreted as an anticooperative behaviour due to the apparently dimeric nature of the protein (Bolognesi et al. 1999). Subsequently, the presence of a dimeric species in VHB has been challenged in an ultracentrifugation investigation thus leaving the biphasic equilibrium ligand binding properties unexplained (Giangiacomo et al. 2001).

A complete reaction scheme (Fig. 16) that takes into account the observed ligand binding profiles has been unravelled on the basis of a set of equilibrium and kinetic measurements carried out on both lipid bound and lipid free HMP. According to Scheme I, the lipid is weakly coordinated to the heme iron and is strongly bound to the non-heme site. Imidazole binding to the heme iron occurs upon displacement (not rate limiting, at least in the case of imidazole) of the weak iron-lipid bond and is entirely accounted for by a typical single site ligand binding process. The non-heme site must possess a very high affinity for the polar lipid head such that it cannot be displaced by heme iron ligands.

In the lipid free protein, the set of imidazole binding kinetics and equilibrium measurements suggested that the ligand might be able to occupy a protein site or cavity next to the heme that allows for rapid exchange with the heme iron. It is envisaged that the incoming ligand is coordinated by the heme iron (k_1'>k_2') and then rapidly partitioned (k_3' ≈

k_3 >1000 s^{-1}) between the metal and the spectroscopically silent non-heme site (Scheme II). This picture is in agreement with the presence of the two sites previously postulated for UFA recognition, i.e. the heme iron site that is capable of coordinating the acyl chain double bond (or cyclopropane ring) and a polar cavity that is necessary for harbouring the polar head of the lipid. Thus, heme iron ligands might be hosted by the polar site in competition with the heme iron in the lipid free HMP.

The main question that arises from the proposed mechanism concerns the nature of the non-heme binding site and its unusual high affinity for the typical ferric heme iron ligands. Attempts to identify the non-heme site by direct X-ray diffraction measurements has failed in that ferric HMP crystals appear to grow only at pH 5.0 and thus under unfavourable conditions for cyanide or imidazole binding (both ligands are protonated). Moreover, HMP crystals were also unstable upon increase in the pH values of the mother solution. Nevertheless, all X-ray diffraction maps thus obtained (including the deposited structure 1gvh, Brookhaven Protein Data Bank) do show electron density in a loop region above the heme pocket comprising residues Asp44-Arg54. The electron density in the loop region has been assigned to a chloride ion although the geometry of the site shares some similarity to typical phosphate coordination regions. In particular, two Arg residues (Arg49 and Arg54) appear to provide a strong positive charge density that allows for coordination of anionic species. It may be envisaged that the loop region, that is endowed with high flexibility, is involved in the coordination of the fatty acid carboxyl and is also able to bind typical heme iron ligands. It is also worth recalling that conformational heterogeneity and hence high flexibility has been postulated to explain the lack of a definite diffraction pattern of the loop region above the heme pocket in ferric ligand free and ligand bound VHB (Tarricone et al. 1997, Bolognesi et al. 1999).

4.2.3 Heme-iron ligand binding properties of ferrous HMP

The effect of the bound lipid on the ferrous protein, although undetectable in the absorption spectra, manifests itself in both CO binding and oxygen release kinetics. It should be mentioned that the description of the CO and oxygen kinetic behaviour is not complete in that no reliable data could be obtained on the oxygen binding process and on the CO release kinetics within the present experimental set up. Thus, the model described for imidazole binding in Scheme II cannot be directly carried over the ferrous protein. Laser photolysis experiments on CO bound HMP revealed very fast and biphasic CO rebinding time courses in the lipid free protein, in agreement with the findings of Gardner and co-workers, (Gardner et al. 2000). In contrast, 10 fold slower and monophasic ligand rebinding kinetics are obtained in the TLE saturated HMP (see Fig. 20). Oxygen release kinetics are also affected by the presence of a bound lipid. Lipid free protein is characterized by a strongly biphasic oxygen release kinetics whose rates and amplitudes are almost superimposable to those obatained on lipid free *Vitreoscilla* Hb (Bolognesi et al. 1999). In contrast, a monoexponential (0.16 s^{-1}) oxygen release process is observed in the lipid saturated protein (Fig. 21).

These experimental observations offer further indications on the interplay between lipid binding and heme iron ligand binding in HMP. The absence of a heme spectroscopic signal in ferrous, lipid bound, HMP is not surprising in that, as observed for most hemoglobins, weak ligands of the ferric heme (*e.g.* fluoride, nitrite, azide) are rapidly released upon iron reduction (Antonini et al. 1971). Nevertheless, given the significant effect on the kinetic parameters of CO and oxygen binding/release, it must be envisaged that the lipid acyl chain is present in the heme pocket thus impairing CO binding and favouring oxygen release processes. Alternatively, the fatty acid might be bound to the non heme site and stabilize a single conformation that reacts slowly with CO and is capable of faster oxygen release (P* conformation of Scheme II). In turn, the lipid free protein must be endowed with a conformational equilibrium between two species to explain the heterogeneity observed in CO binding and oxygen release. These hypothesis (that are not mutually exclusive) may be

reconciled with previous findings based on resonance Raman (Mukai et al. 2001) and infrared spectroscopic (Bonamore et al. 2001) investigations (carried out on the lipid free protein) that envisaged the presence of two distinct conformers in the CO ligated species. The presence of two separate CO stretching frequencies had been attributed to the presence of an "open" and a "closed" conformers (Bonamore et al. 2001). In the "closed" conformer, it has been suggested that iron bound CO is stabilized by the Tyr B10 phenol hydroxyl whereas it is apparently free of constraint in the "open" conformation (Bonamore et al. 2001). Although the reaction Scheme II cannot be easily carried over the ferrous protein, it is tempting to speculate that the "closed" conformation may correspond to the x-P~ species whereas the "open" conformation might be represented by the doubly x-P*~(x) derivative. Interestingly, Scheme II predicts that if the ligand binding rate (k_1') exceeds the rate of ligand exchange between the heme and the non-heme site (k_3'), a biphasic ligand binding kinetics should be observed, as indeed observed for CO binding to the lipid free protein (Gardner et al. 2000).

The kinetics of oxygen release and CO binding have been also investigated for the mutant Glu135- Val in its unique lipid bound derivative. While CO combination is almost superimposable to that obtained for the native protein, the oxygen release is about two orders of magnitude higher (Fig. 22). It is consistent with the loss of the anionic nature of the proximal histidine, which is no more involved in the hydrogen bond network. In fact, the imidazolate property of His F8 becomes lower in Glu135-Val HMP and the electronic density of the heme iron higher. So the affinity for the oxygen decreases in the mutant as the k_{off} decreases and the k_{on} that we measured for the CO remains constant.

4.3 ENZYMATIC ACTIVITY

On the basis of the ligand binding data, we searched for a possible enzymatic activity towards fatty acids or phospholipids. Mono/dioxygenation and/or hydroxylation reactions were screened on several UFAs and CFAs by means of ESI mass spectrometric analysis of fatty acid solutions incubated in the presence of NADH, oxygen and variable amounts of protein (see Table II). The reaction products have been also analysed by GC/MS of the related methyl esthers. In spite of the high affinity for both oxygen and UFAs or CFAs and of the possibly favourable stereochemistry for oxygen addition to the acyl chain, no modifications of the fatty acid were detected under the experimental conditions used (i.e. pH 7.0, 20 °C and NADH as a reductant). Moreover, addition of hydrogen peroxide to the HMP/substrate mixture did not resulted in any modification of the added lipid. In contrast, it was noticed that NADH consumption was increased in the presence of hydrogen peroxide with a rate that was inversely proportional to the oxygen concentration of the buffer. This activity is typical of peroxiredoxins, a family of proteins involved in the physiological response to oxidative stress in microorganisms. Thus, the peroxiredoxin activity of HMP was tested also on a large set of organic alkyl hydroperoxides.

The results obtained indicated clearly that HMP is endowed with a novel enzymatic activity that might be described in the framework of the oxidative stress response of the bacterial cell. In fact, it has been demonstrated that HMP is capable of a very efficient alkyl hydroperoxide reductase activity towards a set of synthetic substrates, namely tert-butyl, cumyl and linoleic acid hydroperoxides. Interestingly, the hydroperoxide reductase activity is higher towards cumyl, tert-butyl and linoleic acid hydroperoxides than towards H_2O_2 thus indicating a preference for highly hydrophobic substrates (Table III). This finding must be analyzed in parallel with recent investigations in which HMP was also shown to interact with bacterial lipid membranes and to be able to bind specifically phospholipids and/or fatty acids within the heme pocket. Taken together, these observations pave the way to a functional role for HMP and possibly other members of the bacterial hemoglobin family: HMP is involved in the repair of peroxidized membrane phospholipids thus reducing hydroperoxides into their corresponding alcohols.

The alkyl hydroperoxide reductase activity is widespread among diverse bacterial species and is thought to represent a major functional response of the cell to oxidative stress. *E. coli* itself posses a protein annotated as alkyl hydroperoxide reductase (AhpC), a NADH-dependent peroxidase that rapidly reduces organic hydroperoxides. AhpC belongs to the peroxiredoxin family (Prxs), that includes thiol-specific antioxidant proteins. Their catalytic cycle is the following: the peroxidatic cysteine attacks the peroxide substrate and is oxidized to a cysteine sulfenic acid; it follows the peroxide decomposition and the exit of the corresponding alcohol. In the second step of the peroxidase reaction the peroxidatic cysteine sulfenic acid is attacked by another cysteine residue within the protein or located at the C-terminus of another subunit in multimeric enzymes. In the last step the so generated disulfide bond is reduced by specific disulfide oxidoreductase (AhpF in *E. coli*) (Wood et al. 2003). Prxs probably overlap to some extent with the better known glutathione peroxidases and catalase, although it has been suggested that their moderate catalytic efficiencies ($\sim 10^5$ $M^{-1}s^{-1}$) compared with those of glutathione peroxidases ($\sim 10^8$ $M^{-1}s^{-1}$) and catalases ($\sim 10^6$ $M^{-1}s^{-1}$) make their importance as peroxidase questionable (Hofmann et al. 2002).

AhpC seems also to be involved in H_2O_2 scavenging (Seaver et al. 2001), although *E. coli* possesses two catalases: HPI and HPII, encoded by katG and katE genes respectively. However, AhpC scavenges low concentration of H_2O_2 very efficiently, while HPI and HPII might act at higher concentration of H_2O_2, against which AhpC is ineffective. So AhpCF peroxiredoxin complex plays a pivotal role in removing hydrogen peroxide in *E. coli* cells under stationary phase conditions (in virtue of a lower K_m value with respect to catalases), whereas it is less efficient as a lipid hydroperoxide scavenger.

The conversion of cumyl hydroperoxide to cumyl alcohol (currently used as a standard for comparing the alkyl hydroperoxide reductase activity among different enzymes) catalysed by HMP occurs at a rate (2564 nmol/min/mg) that is at least two orders of magnitude higher than that measured for the *E. coli* AhpCF complex under similar experimental conditions (Nishiyama et al. 2001) and about 2 fold higher than that measured for the most efficient *Amphibacillus xylanus* peroxiredoxin reductase under saturating condition of AhpC (Niimura et al. 1995). Such a high activity corresponds to a turnover number (mole of substrate per mole of protein) of 110 min^{-1} (see Table III). CO inhibition experiments (Fig. 25, panel B) demonstrate that the activity is heme-linked and is not a spurious effect due to the presence of the highly reactive flavin prosthetic group within the protein. The residual activity observed in HMP in the presence of CO is in fact fully compatible with a competitive inhibition mechanism in which substrate binding is limited kinetically by the rate of CO release from the heme iron.

Simple inspection of the time dependent absorption spectra offers several interesting insights into the mechanism of the alkyl hydroperoxide reductase activity. Analysis of the spectroscopic data of Figs. 26 and 27, together with previous experimental observations on lipid binding to HMP, permits an unequivocal elucidation of the early steps in the mechanism of alkyl hydroperoxide reduction and establishes differences and analogies with classical heme based peroxidase enzymes. Heme peroxidase catalyzes the following global reaction: $2AH_2 + ROOH \rightarrow 2AH\cdot + ROH + H_2O$. The native ferric enzyme reacts with the oxidizing substrate (H_2O_2 or ROOH) to yield compound I, a reactive intermediate with higher formal oxidation state (+5 compared with +3 for the resting enzyme). Then compound I can oxidize a range of reducing substrates by a mechanism involving two sequential single electron steps. That leads the generation of compound II (oxidation state +4) that is reduced to resting enzyme (oxidation state +3) by a second molecule of reducing substrate. In the presence of H_2O_2 in excess another intermediate can be identified, that is compound III (oxygenate derivative with oxidation state +2). Oxygen bound to the ferrous heme in compound III is released as peroxide returning the resting enzyme.

HMP is capable of recognizing the alkyl hydroperoxide moiety due to the highly hydrophobic distal heme pocket and, in the case of peroxidized phospholipids containing

unsaturated fatty acids, has been inferred to be able to adjust the hydrocarbon chain kink in correspondence of the *cis* double bond above the heme iron. Thereafter, binding of the hydroperoxide to the ferrous heme iron occurs with the concomitant two electron reduction and cleavage of the dioxygen bond and consequent formation of a peroxidase-like compound II and an alkyl alcohol. It is important to note that this first step does not imply electron transfer from the flavin to the heme iron but rather a direct two electrons iron oxidation. The fate of the ferryl-oxo compound thus generated is less obvious. Reduction of the ferryl-oxo compund to water and ferric heme with concomitant flavin oxidation and release of the hydroxylphospholipid to the membrane may be hypothesized. Most intriguingly, the active form of the protein, capable of binding a new molecule of substrate, is the ferrous derivative and not the ferric one. In fact, at variance with classical peroxidases, no alkyl hydroperoxide and/or H_2O_2 binding to the heme iron can be detected when the heme iron is in the ferric state. Consistently, ferric HMP is unable to perform monoxygenations typically catalyzed by peroxidases and/or cytochrome p450 on a broad variety of substrates (see Tab. II).

At present, a direct, in vivo, determination of the HMP dependent alkyl hydroperoxide reductase activity still needs to be explored. Nevertheless, a number of experimental observations on HMP expression in response to oxidative stress conditions provide convincing evidence for a genuine physiological role of the protein in the repair of oxidative damage. In particular, it was observed that HMP expression, controlled by the FNR transcription factor, is enhanced under conditions of prolonged oxidative stress such as those imposed by administrating paraquat and other agents generating oxygen reactive species to the culture medium (Membrillo-Hernandez et al. 1999, Anjum et al. 1998). This finding is consistent with HMP being transcribed in a later phase after the oxidative pulse. In fact, whereas the fast response to oxidative stress is governed by enzymes that are directly under the control of the transcription factor OxyR (Nishiyama et al. 2001, Kheng et al. 2001), the late response to oxidative stress involves a web of interactions that ultimately lead to HMP transcription (Anjum et al. 1998). Thus, enzymes involved in hydrogen peroxide scavenging (AhpCF and KatG/E gene products) or DNA protection (Dps gene product) are rendered available as a first barrier against peroxidation whereas HMP and possibly other substrate specific enzymes may play a role in the repair of diverse peroxidized species. In this framework, the link between the reported NO induced (FNR mediated) expression of HMP (Cruz-Ramos et al. 2002) and oxidative stress may reflect another facet of the complex and intimately correlated responses of the bacterial cell to NO and oxygen reactive species. NO induction of enzymes involved in the oxidative stress response is in fact well documented (Ding et al. 2000) and explicit mechanisms that envisage an increase of the alkyl hydroperoxide reductase activity in the presence of NO have been proposed (Bryk et al. 2000). In particular, nitroperoxide species, formed at diffusion limited rate by the reaction of NO with superoxide anion, is known to be a strong promoter of membrane lipid peroxidation (Hogg et al. 1999). Accordingly, NO induced HMP expression, under low oxygen tensions, might well allow a direct (FNR mediated) mechanism for lipid hydroperoxide reduction whereas peroxiredoxins actively scavenge nitroperoxide anions (Bryk et al. 2000).

On the basis of the considerations just presented, HMP and other bacterial hemoglobins would be key enzymes in maintaining the cell membrane integrity at the aerobic/anaerobic interface. Such a hypothesis also provides a plausible explanation for the reported high growth performance of *E. coli* overproducing bacterial hemoglobins under microaerobic environments (Bollinger et al. 2001). Nevertheless, other catalytic options must also be considered in further studies. In fact, lipid hydroperoxide reductase activity might be part of a specific reaction pathway that leads to the formation of lipid hydroperoxide derived active compounds whose functions are, as yet, to be established. It is worth mentioning that in chloroplasts, for instance, unsaturated fatty acid hydroperoxides are converted to signalling molecules by specific cytochrome p450-like proteins such as hydroperoxide lyase and allene oxidase (Baier et al. 1999). Unsaturated fatty acid processing by heme based cycloxygenase

enzymes is also at the basis of the eicosanoids pathway in eukaryotic cells. Intriguingly, cycloxygenases have been proposed to be activated by NO (or by nitroperoxide) in order to trigger the catalytic cycle. In the same way, bacterial hemoglobins might be involved in the (possibly NO driven) processing of phospholipids in the framework of a more complex physiological response.

6. REFERENCES

- Amabile-Cuevas, C. F. and Demple, B. "Molecular characterization of the soxRS genes of *Escherichia coli*: two genes control a superoxide stress regulon" *Nucleic Acid Res.* **19**, 4479-4484 (1991).
- Andrews, S. C., Shipley, D., Keen, J. N., Findlay, J. B., Harrison. P. M. and Guest, J. R. "The haemoglobin-like protein (HMP) of *Escherichia coli* has ferrisiderophore reductase activity and its C-terminal domain shares homology with ferredoxin NADP+ reductases" *FEBS Lett.* **302**, 247-252 (1992).
- Anjum, M. J., Ioannidis, N. and Poole R. K. "Response of the NAD(P)H-oxidising flavohaemoglobin (Hmp) to prolonged oxidative stress and implications for its physiological role in *Escherichia coli*" *FEMS Microbiol. Lett.* **166**, 219-223 (1998).
- Antonini, E. and Brunori, M. in "Hemoglobin and Myoglobin in Their Reactions with Ligands" (Neuberger, A. and Tatum, E. L., Eds.) pp 235-260, North Holland Publishing Co., Amsterdam (1971).
- Baier, M. and Dietz, K. J. "Alkyl hydroperoxide reductases: the way out of the oxidative breakdown of lipids in chloroplasts" *Trends Plant Sci.* **4**, 166-168.
- Balendiran, G. K., Schnutgen, F., Scapin, G., Borchers, T., Xhong, N., Lim, K., Godbut, R., Spener, F. and Sacchettini, J. C. "Crystal structure and thermodynamic analysis of human brain fatty acid-binding protein" (2000) *J. Biol. Chem.* **275**, 27045-27054 (1999).
- Bashford, D., Chothia, C. and Lesk, A. M. "Determinants of a protein fold. Unique features of the globin amino acid sequences" *J Mol Biol.* **196**, 199-216 (1987).
- Bligh, E. G. and Dyer, W. J. "A rapid method of total lipid extraction and purification" *Can. J. Biochem. Physiol.* **37**, 911-917 (1959).
- Boffi, A., Das, T. K., della Longa, S., Spagnolo, C. and Rousseau, D. L. "Pentacoordinate hemin derivatives in sodium dodecyl sulfate micelles: model systems for the assignment of the fifth ligand in ferric heme proteins" *Biophys. J.* **77**, 1143-1149 (1999).
- Boffi, A. and Chiancone, E. "Evaluating cooperativity in dimeric hemoglobins" *Methods Enzymol.* **379**, 55-64 (2004).
- Bollinger, C. J. T., Bailey, J. E. and Kallio, P. T. "Novel hemoglobins to enhance microaerobic growth and substrate utilization in *Escherichia coli*" *Biotechnol. Prog.* **17**, 798-808 (2001).
- Bolognesi, M., Boffi, A., Coletta, M., Mozzarelli, A., Pesce, A., Tarricone, C., and Ascenzi, P. "Anticooperative ligand binding properties of recombinant ferric *Vitreoscilla* homodimeric hemoglobin: a thermodynamic, kinetic and X-ray crystallographic study" *J. Mol. Biol*. **291**, 637-650 (1999).
- Bonamore, A., Chiancone, E. and Boffi, A. "The distal heme pocket of *Escherichia coli* flavohemoglobin probed by infrared spectroscopy" *Biochim. Biophys. Acta* **1549**, 174-178 (2001).
- Brünger, A. T. "A System for X-ray Crystallography and NMR" X-PLOR Version 3.1, Yale University Press, New Haven, CT (1992).
- Bryk, R. Griffin, P. and Nathan, C. "Peroxynitrite reductase activity of bacterial peroxiredoxins" *Nature* **407**, 211-215 (2000).
- Chavez, M. D., Courtney, S. H., Chance, M. R., Kiula, D., Nocek, J., Hoffman, B. M., Friedman, J. M. and Ondrias, M. R. "Structural and functional significance of inhomogeneous line broadening of band III in hemoglobin and Fe-Mn hybrid hemoglobins" *Biochemistry* **29**, 4844-4852 (1990).
- Chiancone, E., Anderson, N. M., Antonini, E., Bonaventura, J., Bonaventura, C., Brunori, M. and Spagnuolo, C. "Effect of heme and non-heme ligands on subunit

dissociation of normal and carboxypeptidase-digested hemoglobin. Gel filtration and flash photolysis studies" *J. Biol. Chem.* **249**, 5689-94 (1974).

- Choi, S., Spiro, T. G., Langry, K. C., Smith, K. M., Budd, D. L. and La Mar, G. M. "Structural correlations and vinyl influences in resonance Raman spectra of protoheme complexes and proteins" *J. Am. Chem. Soc.* **104**, 4345-4351 (1982).
- Corker, H. and Poole, R. K. "Nitric oxide formation by *Escherichia coli*. Dependence on nitrite reductase, the NO-sensing regulator Fnr, and flavohemoglobin Hmp" *J. Biol. Chem.* **278**, 31584-31592 (2003).
- Cruz-Ramos, H., Crak, J., Wu, G., Huges, M. N., Scott, C., Thomson, A. J., Green, J. and Poole, R. K. "NO sensing by FNR: regulation of the *Escherichia coli* NO-detoxifying flavohaemoglobin, Hmp" *EMBO J.* **21**, 3235-3244 (2002).
- da Costa, P. N., Teixeira, M. and Saraiva, L. M. "Regulation of the flavorubredoxin nitric oxide reductase gene in *Escherichia coli*: nitrate repression, nitrite induction, and possible post-transcription control" *FEMS Microbiol Lett.* **218**, 385-393 (2003).
- Ding, H. and Demple, B. "Direct nitric oxide signal transduction via nitrosylation of iron-sulfur centers in the SoxR transcription activator" *Proc. Natl. Acad. Sci. USA* **97**, 5146-5150 (2000).
- Ermler, U., Siddiqui, R.A., Cramm, R., and Friedrich, B. "Crystal structure of the flavohemoglobin from *Alcaligenes eutrophus* at 1.75 A resolution" *EMBO J.* **14**, 6067-6077 (1995).
- Farr, S. B. and Kogoma, T. "Oxidative stress responses in *Escherichia coli* and *Salmonella typhimurium*" *Microbiol. Rev.* **55**, 561-585 (1991).
- Fisher, A. B., Dodia, C., Manevich, Y., Chen J. W. and Feinstein, S.I. "Phospholipid hydroperoxides are substrates for non-selenium glutathione peroxidase" *J. Biol. Chem.* **274**, 21326-21334 (1999).
- Freitas, T. A., Hou, S. and Alam, M. "The diversity of globin-coupled sensors" *FEBS Lett.* **552**, 99-104 (2003).
- Freitas, T. A., Hou, S., Dioum, E. M., Saito, J. A., Newhouse, J., Gonzalez, G., Gilles-Gonzalez, M. A. and Alam, M. "Ancestral hemoglobins in Archaea" *Proc. Natl. Acad. Sci. USA* **101**, 6675-80 (2004).
- Frey, A. D., Bailey, J. E., Kallio, P. T. "Expression of *Alcaligenes eutrophus* flavohemoprotein and engineered *Vitreoscilla* hemoglobin-reductase fusion protein for improved hypoxic growth of *Escherichia coli*" *Appl. Environ. Microbiol.* **66**, 98-104 (2000).
- Frey, A. D., Farres, J., Bollinger, C. J. T. and Kallio, P. T. "Bacterial hemoglobins and flavohemoglobins for alleviation of nitrosative stress in *Escherichia coli*" *Appl. Environ. Microbiol.* **68**, 4835-4840 (2002).
- Gaber, A., Tamoi, M., Takeda, T., Nakano, Y. and Shigeoka, S. "NADPH-dependent glutathione peroxidase-like proteins (Gpx-1, Gpx-2) reduce unsaturated fatty acid hydroperoxides in *Synechocystis* PCC 6803" *FEBS Lett.* **499**, 32-36 (2001).
- Gardner, P. R., Gardner, A. M., Martin, L. A. and Salzman, A. L. "Nitric oxide dioxygenase: an enzymic function for flavohemoglobin" *Proc. Natl. Acad. Sci. USA* **95**, 10378-10383 (1998).
- Gardner, A. M., Martin, L. A., Gardner, P. R., Dou, Y. and Olson, J.S. "Steady-state and transient kinetics of *Escherichia coli* nitric-oxide dioxygenase (flavohemoglobin). The B10 tyrosine hydroxyl is essential for dioxygen binding and catalysis" *J. Biol. Chem.* **275**, 12581-12589 (2000).
- Gardner, A. M., Gessner, C. R. and Gardner P. R. "Regulation of the nitric oxide reduction operon (norRVW) in *Escherichia coli*. Role of NorR and sigma54 in the nitric oxide stress response" *J. Biol. Chem.* **278**, 10081-10086 (2003).

- Giangiacomo, L., Mattu, M., Arcovito, A., Bellenchi, G., Bolognesi, M., Ascenzi, P. and Boffi, A. "Monomer-dimer equilibrium and oxygen binding properties of ferrous *Vitreoscilla* hemoglobin" *Biochemistry* **40**, 9311-9316 (2001).
- Gomes, C. M., Giuffrè, A., Forte, E., Vicente, J. B., Saraiva, L. M., Brunori, M. and Teixeira, M. "A novel type of nitric-oxide reductase. *Escherichia coli* flavorubredoxin" *J. Biol. Chem.* **277**, 25273-25276 (2002).
- Hausladen, A. Gow, A. and Stamler, J. S. "Nitrosative stress: metabolic pathway involving the flavohemoglobin" *Proc. Natl. Acad. Sci. USA* **95**, 14100-14105 (1998).
- Hausladen, A. Gow, A. and Stamler, J. S. "Flavohemoglobin denitrosylase catalyzes the reaction of a nitroxyl equivalent with molecular oxygen" *Proc. Natl. Acad. Sci. USA* **98**, 10108-10112 (2001).
- Hillas, P. J., del Alba, F. S., Oyarzabal, J., Wilks, A. and Ortiz De Mantellano, P. R. "The AhpC and AhpD antioxidant defense system of *Mycobacterium tuberculosis*" *J. Biol. Chem.* **275**, 18801-18809 (2000).
- Hofmann, B. Hecht, H. J. and Flohe, L. "Peroxiredoxins" *Biol. Chem.* **383**, 347-364 (2002).
- Hogg, N. and Kalyanaraman, B. "Nitric oxide and lipid peroxidation" *Biochem. Biophys. Acta* **1411**, 378-384 (1999).
- Hou, S., Freitas, T., Larsen, R. W., Piatibratov, M., Sivozhelezov, V., Yamamoto, A., Meleshkevitch, E. A., Zimmer, M., Ordal, G. W. and Alam, M. "Globin-coupled sensors: a class of heme-containing sensors in Archaea and Bacteria" *Proc. Natl. Acad. Sci. USA* **98**, 9353-9358 (2001).
- Hu, S., Smith, K. M. and Spiro, T. G. "Assignment of protoheme resonance Raman spectrum by heme labeling in myoglobin" *J. Am. Chem. Soc.* **118**, 12638-12646 (1996).
- Kallio, P. T., Kim, D. J., Tsai, P. S. and Bailey, J. E. "Intracellular expression of *Vitreoscilla* hemoglobin alters *Escherichia coli* energy metabolism under oxygen-limited conditions" *Eur. J. Biochem.* **219**, 201-208 (1994).
- Khang, Y. H., Kim, I. W., Hah, Y. R., Hwangbo, J. H. and Kang, K. K. "Fusion protein of *Vitreoscilla* hemoglobin with D-amino acid oxidase enhances activity and stability of biocatalyst in the bioconversion process of cephalosporin C" *Biotechnol. Bioeng.* **82**, 480-488 (2003).
- Kim, S. O., Orii, Y., Lloyd, D., Hughes, M. N. and Poole, R. K. "Anoxic function for the *Escherichia coli* flavohaemoglobin (Hmp): reversible binding of nitric oxide and reduction to nitrous oxide" *FEBS Lett.* **445**, 389-394 (1999).
- Kim, Y. K., Kang, D. G., Choi, S. S., Kim, J. H., Chung J. C. and Cha H. J. "Enhancement of 2,4-dinitrotoluene biodegradation by *Burkholderia* Sp. in sand bioreactors using bacterial hemoglobin technology" *Biodegradation* **15**, 161-171 (2004).
- Korner, H., Sofia, H. J. and Zumft, W. G. "Phylogeny of the bacterial superfamily of Crp-Fnr transcription regulators: exploiting the metabolic spectrum by controlling alternative gene programs" *FEMS Microbiol. Rev.* **27**, 559-592 (2003).
- Lewis, T., Nichols, P. D. and Mc Meekin, T. A. "Evaluation of extraction methods for recovery of fatty acids from lipid-producing microheterotrophs" *J. Microbiol. Methods* **43**, 107-116 (2000).
- Lin, J.M., Stark, B. C. and Webster, D. A. "Effects of *Vitreoscilla* hemoglobin on the 2,4-dinitrotoluene (2,4-DNT) dioxygenase activity of *Burkholderia* and on 2,4-DNT degradation in two-phase bioreactors" *J. Ind. Microbiol. Biotechnol.* **30**, 362-368 (2003).
- Loida, P. J. and Sligar, S. G. "Molecular recognition in cytochrome P-450: mechanism for the control of uncoupling reactions" *Biochemistry* **32**, 11530-11538 (1993).

- Membrillo-Hernandez, J., Ioannidis, N. and Poole, R. K. "The flavohaemoglobin (HMP) of *Escherichia coli* generates superoxide in vitro and causes oxidative stress in vivo" *FEBS Lett.* **382**, 141-144 (1996).
- Membrillo-Hernandez, J., Kim, S. O., Cook, G. M. and Poole, R. K. "Paraquat regulation of hmp (flavohemoglobin) gene expression in *Escherichia coli* K-12 is SoxRS independent but modulated by sigma S" *J. Bacteriol.* **179**, 3164-3170 (1997).
- Membrillo-Hernandez, J., Coopamah, M. D., Channa, A., Hughes, M. N. and Poole, R. K. "A novel mechanism for upregulation of the *Escherichia coli* K-12 hmp (flavohaemoglobin) gene by the 'NO releaser', S-nitrosoglutathione: nitrosation of homocysteine and modulation of MetR binding to the glyA-hmp intergenic region" *Mol. Microbiol.* **29**, 1101-1112 (1998).
- Membrillo-Hernandez, J., Coopamah, M. D., Anjum, M. F., Stevanin, T. M., Kelly, A., Hughes, M. N. and Poole, R. K. "The flavohemoglobin of *Escherichia coli* confers resistance to a nitrosating agent, a "Nitric oxide Releaser," and paraquat and is essential for transcriptional responses to oxidative stress" *J. Biol. Chem.* **274**, 748-754 (1999).
- Minas, W., Bunker, P., Kallio, P. T. and Bailey, J. E. "Improved erythromycin production in a genetically engineered industrial strain of *Saccharopolyspora erythraea*" *Biotechnol. Prog.* **14**, 561-566 (1998).
- Mukai, M., Mills, C. E., Poole, R. K., Yeh, S. R. "Flavohemoglobin, a globin with a peroxidase-like catalytic site" *J. Biol. Chem.* **276**, 7272-7277 (2001).
- Nasr, M. A., Hwang, K. W., Akbas, M., Webster, D. A. and Stark, B. C. "Effects of culture conditions on enhancement of 2,4-dinitrotoluene degradation by *Burkholderia* engineered with the *Vitreoscilla* hemoglobin gene" *Biotechnol. Prog.* 17, 359-361 (2001).
- Niimura, Y., Poole, L. B. and Massey, V. "*Amphibacillus xylanus* NADH oxidase and *Salmonella typhimurium* alkyl-hydroperoxide reductase flavoprotein components show extremely high scavenging activity for both alkyl hydroperoxide and hydrogen peroxide in the presence of *S. typhimurium* alkyl-hydroperoxide reductase 22-kDa protein component" *J. Biol. Chem.* **270**, 25645-25650 (1995).
- Nishiyama, Y., Massey, V., Takeda, K., Kawasaki, S., Sato, J., Watanabe, T. and Niimura, Y. "Hydrogen peroxide-forming NADH oxidase belonging to the peroxiredoxin oxidoreductase family: existence and physiological role in bacteria" *J. Bacteriol.* **183**, 2431-2438 (2001).
- Nunoshiba, T., Hidalgo, E., Amabile-Cuevas, C. F. and Demple, B. "Two-stage control of an oxidative stress regulon: the *Escherichia coli* SoxR protein triggers redox-inducible expression of the soxS regulatory gene" *J. Bacteriol.* **174**, 6054-6060 (1992).
- Ollesch, G., Kaunzinger, A., Juchelka, D., Schubert-Zsilavec, M. and Ermler, U. "Phospholipid bound to the flavohemoprotein from *Alcaligenes eutrophus*" *Eur. J. Biochem.* **262**, 396-405 (1999).
- Otwinowski, Z. and Minor, W. "Processing of X-ray diffraction data collected in oscillation mode" *Methods Enzymol.* **276,** 307–326 (1997).
- Park, K. W., Kim, K. J., Howard, A. J., Stark, B. C. and Webster, D. A. "*Vitreoscilla* hemoglobin binds to subunit I of cytochrome bo ubiquinol oxidases" *J. Biol. Chem.* **277**, 33334-33337 (2002).
- Pathania, R., Navani, N. K., Rajamohan, G. and Dikshit, K. L. "*Mycobacterium tuberculosis* hemoglobin HbO associates with membranes and stimulates cellular respiration of recombinant *Escherichia coli*" *J. Biol. Chem.* **277**, 15293, 15302 (2002).
- Peterson, E. S., Huang, S., Miller, L. M., Vidugiris, G., Kloek, A. P., Goldberg, D. E., Chance, M. R., Wittenberg, J. B. and Friedman, J. M. "A comparison of functional

and structural consequences of the tyrosine B10 and glutamine E7 motifs in two invertebrate hemoglobins (*Ascaris suum* and *Lucina pectinata*)" *Biochemistry* **36**, 13110-13121 (1997).

- Poole, R. K., Anjum, M. F., Membrillo-Hernandez, J., Kim, S. O., Hughes, M. N. and Stewart, V. "Nitric oxide, nitrite, and Fnr regulation of hmp (flavohemoglobin) gene expression in *Escherichia coli* K-12" *J. Bacteriol.* **178**, 5487-5492 (1996).
- Poole, R. K.and Hughes, M. N. "New functions for the ancient globin family: bacterial responses to nitric oxide and nitrosative stress" *Mol Microbiol.* **36**, 775-783 (2000).
- Ramandeep, Hwang, K.W., Raje, M., Kim, K.J., Stark, B.C., Dikshit, K.L. and Webster, D.A. "*Vitreoscilla* hemoglobin. Intracellular localization and binding to membranes" *J. Biol. Chem*. **276**, 24781-24789 (2001).
- Seaver, L. C. and Imlay, J. A. "Alkyl hydroperoxide reductase is the primary scavenger of endogenous hydrogen peroxide in *Escherichia coli*" *J. Bacteriol.* **183**, 7173-7181 (2001).
- Smulevich, G. S., Hu, S., Rodgers, K. R., Goodin, D. B., Smith, K. M. and Spiro, T. G. "Heme-protein interactions in CcP revealed by site-directed mutagenesis and resonance Raman spectra of isotopically-labeled hemes" *Biospectroscopy* **2**, 365-375 (1996).
- Spiro, T. G. "Resonance Raman spectroscopy as a probe of heme protein structure and dynamics" *Adv. Protein Chem.***37**, 111-159 (1985).
- Takeda, K., Nishiyama, Y., Yoda, K., Watanabe, T., Nimura-Matsune, K., Mura, K., Tokue, C., Katoh, T., Kawasaki, S. and Niimura, Y. "Distribution of Prx-linked hydroperoxide reductase activity among microorganisms" *Biosci. Biotechnol. Biochem.* **68**, 20-27 (2004).
- Tarricone, C., Galizzi, A., Coda, A., Ascenzi, P., and Bolognesi, M. "Unusual structure of the oxygen-binding site in the dimeric bacterial hemoglobin from *Vitreoscilla sp*" *Structure* **14**, 497-507 (1997).
- Urgun-Demirtas, M., Pagilla, K. R., Stark, B. C.and Webster, D. "Biodegradation of 2-chlorobenzoate by recombinant *Burkholderia cepacia* expressing *Vitreoscilla* hemoglobin under variable levels of oxygen availability" *Biodegradation* **14**, 357-365 (2003).
- Vasudevan, S. G., Armarego, W. L., Shaw, D. C., Lilley, P. E., Dixon, N. E. and Poole, R. K. "Isolation and nucleotide sequence of the hmp gene that encodes a haemoglobin-like protein in *Escherichia coli* K-12" *Mol. Gen. Genet.* **226**, 49-58 (1991).
- Wilmot, C. M., Sjogren, T., Carlsson, G. H., Berglund, G.I. and Hajdu, J. "Defining redox state of X-ray crystal structures by single-crystal ultraviolet-visible microspectrophotometry" *Methods Enzymol.* **353**, 301-318 (2002).
- Wittenberg, J. B., Bolognesi, M., Wittenberg, B. A. and Guertin, M. "Truncated hemoglobins: a new family of hemoglobins widely distributed in bacteria, unicellular eukaryotes, and plants" *J. Biol. Chem.* **277**, 871-874 (2002).
- Wood, Z. A., Schröder, E., Harris, J. R. and Poole L. B. "Structure, mechanism and regulation of peroxiredoxins" *Trends Biochem. Sci.* **28**, 32-40 (2003).
- Wu, G., Wainwright, L. M. and Poole, R.K. "Microbial globins" *Adv Microb Physiol.* **47**, 255-310 (2003).
- Zheng, M., Wang, X., Templeton, L. J., Smulski, D. R., La Rossa, R. A. and Storz, G. "DNA microarray-mediated transcriptional profiling of the *Escherichia coli* response to hydrogen peroxide" *J. Bacteriol.* **138**, 4562-4570 (2001).